Symmetry-Breaking Bifurcations for Compartmental Reaction Kinetics Coupled by Two Bulk Diffusing Species with Comparable Diffusivities in 2-D

Merlin Pelz[1] and Michael Ward[2]

[1,2]University of British Columbia, Vancouver, Canada

December 1, 2022

Abstract

For a 2-D coupled PDE-ODE bulk-cell model, we investigate symmetry-breaking bifurcations that can emerge when two bulk diffusing species are coupled to two-component nonlinear intracellular reactions that are restricted to occur only within a disjoint collection of small circular compartments, or "cells", of a common small radius that are confined in a bounded 2-D domain. Outside of the union of these cells, the two bulk species with comparable diffusivities and bulk degradation rates diffuse and globally couple the spatially segregated intracellular reactions through Robin boundary conditions across the cell boundaries, which depend on certain membrane reaction rates. In the singular limit of a small common cell radius, we construct steady-state solutions for the bulk-cell model and formulate a nonlinear matrix eigenvalue problem that determines the linear stability properties of the steady-states. For a certain spatial arrangement of cells for which the steady-state and linear stability analysis become highly tractable, we construct a symmetric steady-state solution where the steady-states of the intracellular species are the same for each cell. As regulated by the ratio of the membrane reaction rates on the cell boundaries, we show for various specific prototypical intracellular reactions, and for a specific two-cell arrangement, that our 2-D coupled PDE-ODE model admits symmetry-breaking bifurcations from this symmetric steady-state, leading to linearly stable asymmetric patterns, even when the bulk diffusing species have comparable or possibly equal diffusivities. Overall, our analysis shows that symmetry-breaking bifurcations can occur without the large diffusivity ratio requirement for the bulk diffusing species as is well-known from a Turing stability analysis from a spatially uniform steady-state for typical two-component activator-inhibitor systems. Instead, for our theoretical compartmental-reaction diffusion bulk-cell model, our analysis shows that the emergence of stable asymmetric steady-states can be controlled by the ratio of the membrane reaction rates for the two species. Bifurcation theoretic results for symmetric and asymmetric steady-state patterns obtained from our asymptotic theory are confirmed with full numerical PDE simulations.

1 Introduction

A central issue in many chemical and biological systems that involve the coupling of diffusive processes and nonlinear reactions is to determine conditions for which spatio-temporal patterns can form from either a patternless or a pre-patterned state. In a pioneering theoretical study, Alan Turing [58] established that diffusing morphogens with different diffusivities can destablilize a spatially uniform and stable steady-state of the nonlinear reaction kinetics. As applied to two-component activator-inhibitor reaction-diffusion (RD) systems, this Turing stability analysis shows that a sufficiently large diffusivity ratio is typically needed to obtain spatial pattern formation from the destabilization of a spatially uniform state, unless the nonlinear reaction kinetics are finely tuned (cf. [44], [1], [8]). For certain chemical systems, this large diffusivity ratio requirement needed for pattern formation may be feasible to achieve in situations where one of the chemical species can bind to a substrate, which has the consequence of reducing the *effective* diffusivity of this species (cf. [33], [10]). However, in many cellular processes related to developmental biology and morphogenesis, the theoretical large diffusivity ratio threshold needed for freely diffusing morphogens to create symmetry-breaking patterns is often unrealistic as different small molecules typically have very comparable diffusivities (cf. [39], [51]). In [39], various modifications of the simple "freely diffusing" morphogen paradigm such as, *facilitated diffusion*, *transient binding*, *immobilization* and *transcytosis*,

among others, have been postulated to play a central role in specific applications of diffusive transport at the cellular level. Qualitatively, the postulated overall effect of these mechanisms is to modify an *effective* diffusivity ratio of the morphogens, which can, therefore, lead to the emergence of spatial patterns and symmetry-breaking behavior in cellular processes related to developmental biology and early morphogenesis (cf. [51]).

As a result, one key long-standing theoretical question in RD theory is how to modify the two-component RD paradigm so as to robustly generate stable spatial patterns from a spatially homogeneous state when the time scales for diffusion of the interacting species are comparable. By including an additional non-diffusible component, which roughly models either membrane-bound proteins or an immobile chemically active substrate, it has been shown (cf. [43], [29], [30]) that this "$2+1$" extension of the two-component RD framework can yield stable spatial patterns even when the two diffusible species have a common diffusivity. In another direction, which is based on graph-theoretic properties associated with nonlinear reactions between multiple species that are either immobile or freely diffusing, it has been shown that with certain activating and inhibiting feedback relations in the chemical kinetics, spatial patterns can form without the large diffusivity ratio requirement (cf. [38], [9], [32]). More recently, the authors in [23] have revealed that in random, multi-component, RD systems the required diffusivity threshold for pattern formation typically decreases as the number of interacting and diffusing species increases.

From a theoretical viewpoint, in specific applications where a large diffusivity ratio is a realistic assumption, it has been shown both analytically and from numerical simulations (cf. [59], [60], [24], [25]) that two-component RD systems admit a wide range of spatially localized patterns and instabilities that occur in the "far-from-equilibrium" regime, far from where a Turing linear stability analysis will provide any insight into pattern-forming properties.

The goal of this paper is to formulate and quantitatively analyze a new theoretical model in a 2-D setting that robustly leads to pattern formation even when the two diffusing species have a comparable or equal diffusivity. More specifically, we analyze symmetry-breaking pattern formation for a 2-D PDE-ODE bulk-cell RD model in which spatially segregated localized reaction compartments, referred to as "cells", are coupled to a two-component linear bulk diffusion field with constant bulk degradation rates. In the cells, which are assumed to have a common radius that is small compared to the domain length-scale and the inter-cell distances, two-component intracellular activator-inhibitor reaction kinetics are specified. The intraceullar species undergo an exchange with the two bulk species across the cell boundaries, as mediated by membrane reaction rates in a Robin boundary condition that is specified on each cell boundary. The two extracellular diffusing bulk species, with comparable diffusivities and degradation rates, provide the mechanism that couples the nonlinear intracellular reactions that occur in the union of the spatially segregated cells. We refer to this modeling framework as a **compartmental-reaction diffusion system.**

The numerical implementation of our theoretical analysis for this model for various specific intracellular reaction kinetics reveals that it is the ratio of the reaction rate of the inhibitor component to that of the activator component on the compartment boundaries that plays a central role in the initiation of symmetry-breaking bifurcations of a symmetric steady-state. The magnitude of this ratio ultimately controls whether linearly stable asymmetric steady-states for the bulk-cell model can occur even when the bulk diffusivities are comparable or equal. The bifurcation threshold condition for this key membrane reaction rate ratio parameter is distinct from the usual large diffusivity ratio threshold that is required for pattern formation from a spatially uniform state for typical two-component activator-inhibitor RD systems (cf. [37], [31]). We emphasize that our linear stability analysis predicting symmetry-breaking bifurcations for the bulk-cell model, as regulated by the membrane reaction rate ratio, is significantly more challenging than performing a simple Turing stability analysis [58] since it is based on the linearization of the bulk-cell model around a *spatially non-uniform* symmetric steady-state. In our previous 1-D study [45], where nonlinear reactions were restricted either to domain boundaries or at lattice site on a 1-D periodic chain, it has been shown for some specific nonlinear kinetics that symmetry-breaking bifurcations can occur from a symmetric steady-state when the ratio of membrane reaction rates exceeds a threshold.

We remark that our 2-D study, and related 1-D analysis in [45], is largely inspired by the agent-based numerical computations in [49] where it was shown that nonlinear kinetic reactions restricted to lattice sites on a 2-D lattice can generate stable Turing-type spatial patterns when coupled through a spatially discretized two-component bulk diffusion field in which the two diffusible species have a comparable diffusivity.

In a broader context, the study of novel pattern-forming properties associated with compartmentalized reactions interacting through a passive bulk diffusion field originates from the 1-D analysis in [17] for the FitzHugh-

Nagumo model and the bulk-membrane analysis of [34] in disk-shaped domains. In a 1-D context, and with one bulk diffusing species, this compartmental-reaction diffusion system modeling paradigm has been shown to lead to triggered oscillatory instabilities for various reaction kinetics involving conditional oscillators (cf. [19], [21], [18]). Amplitude equations characterizing the local branching behavior for these triggered oscillations have been derived in [41] using a weakly nonlinear analysis. Applications of this framework have been used to model intracellular polarization and oscillations in fission yeast (cf. [61], [62]). In a 2-D domain, similar bulk-cell models, but with only one diffusing bulk species, have been formulated and used to model quorum-sensing behavior (cf. [20], [28], [50], [16]). With regards to bulk-membrane RD models in a multi-spatial dimensional context, where nonlinear kinetics are restricted to the membrane, the associated pattern-forming properties have been studied both theoretically (cf. ([48], [11], [36], [35], [40]), and for some specific biological applications (cf. [6], [46], [47], [52], [42]).

The outline of this paper is as follows. In §2 we formulate our bulk-cell model and use a singular perturbation approach in the limit of a small common cell radius to derive a nonlinear algebraic system characterizing all steady-state solutions of the model. In §3 we show that the discrete eigenvalues of the linearization of the bulk-cell model around a steady-state solution are determined by a root-finding condition on a nonlinear matrix eigenvalue problem. For a certain type of spatial configuration of the cells, the bulk-cell model is shown to admit a symmetric steady-state solution in which the steady-states of the intracellular reactions are identical. The possibility of symmetry-breaking bifurcations along this symmetric steady-state solution branch, leading to the existence of linearly stable asymmetric patterns, are analyzed by applying solution path continuation software to our bifurcation-theoretic analytical results. For a certain two-cell configuration in the unit disk, and for either Gierer-Meinhardt [15], Rauch-Millonas [49], or FitzHugh-Nagumo [17] intracellular reactions, we show in §4 that it is the magnitude of the ratio of the reaction rates for the two bulk species on the cell membranes that controls whether linearly stable asymmetric patterns can bifurcate from the symmetric steady-state. Our theoretical predictions of symmetry-breaking behavior, leading to stable asymmetric steady-states even when the two bulk species have comparable or equal diffusivities, are confirmed from full PDE numerical simulations. For a closely-spaced arrangement of cells as is typical in biological tissues, and where our asymptotic theory no longer applies, the PDE numerical simulations shown in §4.4 illustrate that symmetry-breaking bifurcations can still be controlled by the reaction rate ratio on the cell boundaries. In particular, our numerical results suggest that such bifurcations occur with a smaller membrane reaction-rate ratio than for the situation where the cells are more spatially segregated. In §5 we discuss our theoretical results in a wider context, and suggest a few open directions.

2 Compartmental-reaction diffusion system in 2-D

2.1 Model formulation

We consider a bounded 2-D domain with length scale L, denoted by $\Omega^L \subset \mathbb{R}^2$, that contains m disconnected circular compartments Ω_j^L, for $j \in \{1, ..., m\}$, referred to as "cells". We will assume that these cells have a common radius that is small in comparison with the length scale L of the domain. The bulk or extracellular medium is the region $\Omega^L \setminus \bigcup_{j=1}^m \Omega_j^L$.

In the bulk we assume that there are two extracellularly diffusing and degrading chemical species with concentrations U and V. These messenger molecules are synthesized on the "cell" membranes through the interaction with two corresponding intracellular species M_j and H_j. With the molecule counts $\mathfrak{U}, \mathfrak{V}, \mathfrak{M}_j$ and $\mathfrak{H}_j$ corresponding to respectively U, V, M_j and H_j, the chemical equations are

$$\mathfrak{U} \underset{\beta_U}{\overset{\beta_U}{\rightleftharpoons}} \mathfrak{M}_j\,, \qquad \mathfrak{V} \underset{\beta_V}{\overset{\beta_V}{\rightleftharpoons}} \mathfrak{H}_j\,. \tag{2.1}$$

Here we made the assumption that the exponential forward reaction rates equal the backward reaction rates and that all compartments are identical in that they have common membrane reaction rates. The intra-compartmental species, in turn, are produced by certain reaction kinetics, denoted by $f(M, H)$ and $g(M, H)$, that are assumed to be identical in each compartment.

More precisely, in dimensional variables, our bulk-cell coupled model is

$$\text{bulk} \quad \begin{cases} \partial_T U = D_U\,\Delta_X U - \kappa_U\,U\,, & \mathbf{X}\in\Omega^L\backslash\bigcup_{j=1}^m\Omega_j^L\,, \\ \partial_T V = D_V\,\Delta_X V - \kappa_V\,V\,, & \mathbf{X}\in\Omega^L\backslash\bigcup_{j=1}^m\Omega_j^L\,, \\ \partial_{\tilde{n}_X} U = \partial_{\tilde{n}_X} V = 0\,, & \mathbf{X}\in\partial\Omega^L\,, \qquad \text{(Neumann condition)} \end{cases} \tag{2.2a}$$

$$\text{reaction fluxes} \quad \begin{cases} D_U\,\partial_{n_{j,X}} U = \beta_{U,1}\,U - \beta_{U,2}\,M_j\,, & \mathbf{X}\in\partial\Omega_j^L\,, \qquad \text{(Robin condition)} \\ D_V\,\partial_{n_{j,X}} V = \beta_{V,1}\,V - \beta_{V,2}\,H_j\,, & \mathbf{X}\in\partial\Omega_j^L\,, \end{cases} \tag{2.2b}$$

$$\text{compartments} \quad \begin{cases} \frac{d}{dT}M_j = \kappa_R\,\mu_c\,f\left(\frac{1}{\mu_c}M_j,\frac{1}{\mu_c}H_j\right) + \int_{\partial\Omega_j^L}(\beta_{U,1}\,U - \beta_{U,2}\,M_j)\,dS_X\,, \\ \frac{d}{dT}H_j = \kappa_R\,\mu_c\,g\left(\frac{1}{\mu_c}M_j,\frac{1}{\mu_c}H_j\right) + \int_{\partial\Omega_j^L}(\beta_{V,1}\,V - \beta_{V,2}\,H_j)\,dS_X \quad \text{(reaction kinetics)}\,, \end{cases} \tag{2.2c}$$

with $j\in\{1,...,m\}$ and where $n_{j,X}$ is the outward unit normal vector to Ω_j^L while $\tilde{n}_X$ is the outward unit normal vector to Ω^L. The diffusivities (diffusion coefficients) for U and V are D_U and D_V, and U and V are degrading in the bulk with exponential rate constants κ_U and κ_V, respectively. The exponential reaction rates on the compartment boundaries are β_U and β_V with corresponding rates $\beta_{U,1}$ and $\beta_{V,1}$ per area times length and $\beta_{U,2}$ and $\beta_{V,2}$ per length and time units, and μ_c is a normalizing constant for the intracellular species. Lastly, κ_R is a dimensional reaction rate for the intracellular reactions.

In Appendix A we non-dimensionalize (2.2) to obtain the dimensionless PDE-ODE model

$$\text{bulk} \quad \begin{cases} \partial_t u = D_u\Delta u - \sigma_u u\,, & \mathbf{x}\in\Omega\backslash\bigcup_{j=1}^m\Omega_j\,, \\ \partial_t v = D_v\Delta v - \sigma_v v\,, & \mathbf{x}\in\Omega\backslash\bigcup_{j=1}^m\Omega_j\,, \\ \partial_{\tilde{n}} u = \partial_{\tilde{n}} v = 0\,, & \mathbf{x}\in\partial\Omega\,, \end{cases} \tag{2.3a}$$

$$\text{reaction fluxes} \quad \begin{cases} \varepsilon D_u\partial_{n_j} u = d_1^u u - d_2^u\mu_j\,, & \mathbf{x}\in\partial\Omega_j\,, \\ \varepsilon D_v\partial_{n_j} v = d_1^v v - d_2^v\eta_j\,, & \mathbf{x}\in\partial\Omega_j\,, \end{cases} \tag{2.3b}$$

$$\text{compartments} \quad \begin{cases} \frac{d\mu_j}{dt} = f(\mu_j,\eta_j) + \frac{1}{\varepsilon}\int_{\partial\Omega_j}(d_1^u u - d_2^u\mu_j)\,dS\,, \\ \frac{d\eta_j}{dt} = g(\mu_j,\eta_j) + \frac{1}{\varepsilon}\int_{\partial\Omega_j}(d_1^v v - d_2^v\eta_j)\,dS\,, \end{cases} \tag{2.3c}$$

for $j\in\{1,\dots,m\}$. Here n and $\tilde{n}$ are the outward unit normal vectors to Ω_j and Ω, respectively, and we have dropped the label "x" for Δ and the outward unit normal vectors. In (2.3), the compartments are disks of a common radius $\varepsilon\ll 1$ centered at $\mathbf{x}_j\in\Omega$, i.e. $\Omega_j\equiv\{\mathbf{x}\,|\,|\mathbf{x}-\mathbf{x}_j|\le\varepsilon\}$. We will refer to d_1^u, d_1^v, d_2^u, and d_2^v as dimensionless membrane reaction rates. An illustration of the bulk-cell model is shown in Figure 1.

We will use strong localized perturbation theory [60] to construct the steady-state solutions of (2.3) and to analyze their linear stability properties in the asymptotic limit $\varepsilon\ll 1$ and under the assumption that m circular cells are well-separated in the sense that the cell centers satisfy $|\mathbf{x}_i-\mathbf{x}_j|=\mathcal{O}(1)$, for $i,j\in\{1,...,m\}$ and $i\neq j$.

2.2 Asymptotic construction of the steady-states

Our main goal is to construct a symmetric steady-state solution for (2.3) in which the concentration of each species is the same inside and in the local vicinity of each compartment. We will show below that even when the bulk diffusing species have comparable diffusivities this symmetric steady-state is unstable to symmetry-breaking perturbations that occur beyond a pitchfork bifurcation point associated with the membrane reaction rate ratio $\rho\equiv d_1^v/d_1^u = d_2^v/d_2^u$. This leads to the existence of linearly stable asymmetric steady-state solutions to (2.3).

In the absence of diffusion, the ODE system for the intra-compartmental species is decoupled from the bulk medium and reduces to

$$\dot{\mu}(t) = f(\mu,\eta)\,, \qquad \dot{\eta}(t) = g(\mu,\eta)\,. \tag{2.4}$$

Let (μ_e,η_e) be an equilibrium point for (2.4) and label $F(\mu,\eta)\equiv(f(\mu,\eta),g(\mu,\eta))$. For a specific parameter set, the linear stability property of the equilibrium state is characterized by whether the eigenvalues λ of the Jacobian matrix $DF(\mu_e,\eta_e)$ have positive (unstable, exponentially growing perturbations) or negative (stable, exponentially

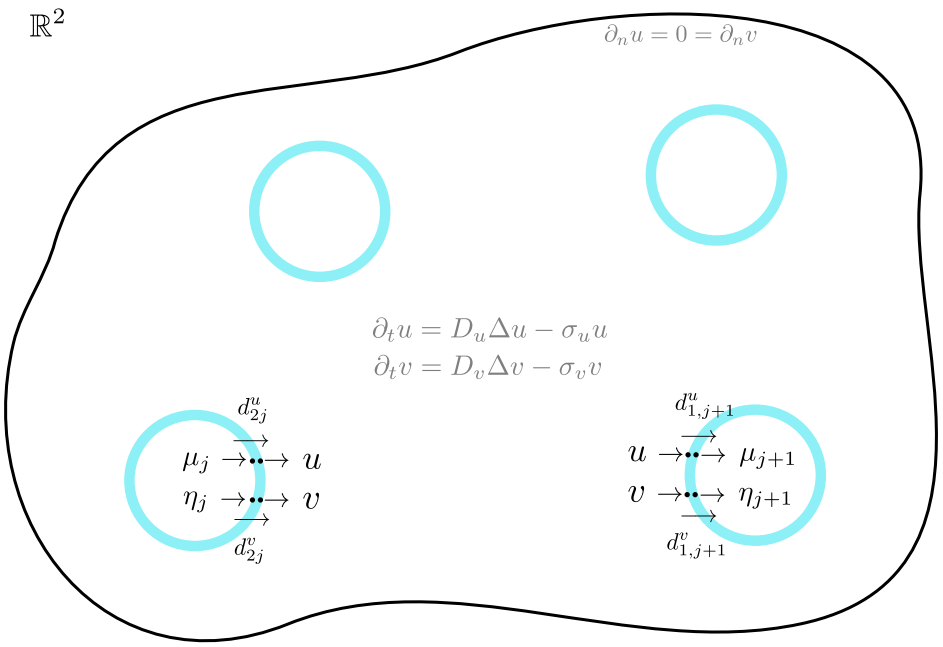

Figure 1: A bounded domain with four diffusion-coupled cells. In the j^{th} cell, activator-inhibitor reaction kinetics occur for the activator μ_j and inhibitor η_j. Across the cell membrane, there is an exchange between the intracellular and bulk species. In the bulk, u and v diffuse and undergo degradation. The cells are assumed to be small but are drawn larger here for illustration only.

decaying perturbations) real parts $\text{Re}(\lambda)$. However, when there is bulk diffusion and the compartments are coupled through the bulk, the the steady-state solution in the compartments depends on the bulk diffusivities, the membrane reaction rates, and the spatial configuration of the cells.

We now use the method of matched asymptotic expansions to construct steady-state solutions for (2.3). In the j^{th} inner region, defined within an $\mathcal{O}(\varepsilon)$ neighborhood of the boundary of the j^{th} cell, we introduce the local variables $\mathbf{y}_j = \varepsilon^{-1}(\mathbf{x} - \mathbf{x}_j)$, $U_j(\mathbf{x}) = U_j(\varepsilon \mathbf{y}_j + \mathbf{x}_j)$, and $V_j(\mathbf{x}) = V_j(\varepsilon \mathbf{y}_j + \mathbf{x}_j)$, where $p_j \equiv |\mathbf{y}_j|$. Upon writing the steady-state of (2.3a) in terms of the inner variables, for $\varepsilon \to 0$ the steady-state problem in the j^{th} inner region is $\Delta U_j = 0$ and $\Delta V_j = 0$, for $p_j \geq 1$, subject to $D_u \, \partial_{p_j} U_j = d_1^u U_j - d_2^u \mu_j$ and $D_v \, \partial_{p_j} V_j = d_1^v V_j - d_2^v \eta_j$ on $p_j = 1$. The radially symmetric solutions to these problems are

$$U_j(p_j) = A_j^u \log p_j + \frac{1}{d_1^u} \left(D_u \, A_j^u + d_2^u \mu_j \right) , \qquad V_j(p_j) = A_j^v \log p_j + \frac{1}{d_1^v} \left(D_v \, A_j^v + d_2^v \eta_j \right) , \tag{2.5}$$

for $j \in \{1, \ldots, m\}$, where A_j^u and A_j^v for $j = 1, \ldots, m$ are constants to be determined. Upon substituting (2.5) into the steady-state problem of (2.3c), we obtain for the j^{th} cell that

$$f(\mu_j, \eta_j) + 2\pi D_u \, A_j^u = 0 \, , \qquad g(\mu_j, \eta_j) + 2\pi D_v \, A_j^v = 0 \, , \qquad j \in \{1, \ldots, m\} \, . \tag{2.6}$$

Next, we must determine A_j^u and A_j^v by matching the far-field behavior of the inner solutions (2.5) to the outer solutions defined in the bulk region.

In the limit $\varepsilon \to 0$, in the bulk region the compartments formally shrink to points and from the far-field behavior of (2.5), when written in outer variables, we obtain that the steady-state bulk species U satisfies

$$\Delta U - \omega_u^2 \, U = 0 \, , \quad \mathbf{x} \in \Omega \setminus \{\mathbf{x}_1, \ldots, \mathbf{x}_m\} \, ; \qquad \partial_n U = 0 \, , \quad \mathbf{x} \in \partial\Omega \, ; \tag{2.7a}$$

$$U \sim A_j^u \log |\mathbf{x} - \mathbf{x}_j| + \frac{A_j^u}{\nu} + \frac{1}{d_1^u} (D_u A_j^u + d_2^u \mu_j) \, , \quad \text{as} \quad \mathbf{x} \to \mathbf{x}_j \, , \qquad j \in \{1, \ldots, m\} \, , \tag{2.7b}$$

where $\nu \equiv -1/\log\varepsilon \ll 1$ and $\omega_u \equiv \sqrt{\sigma_u/D_u}$. Similarly, with $\omega_v \equiv \sqrt{\sigma_v/D_v}$, for the bulk species V we have that

$$\Delta V - \omega_v^2 V = 0\,, \quad \mathbf{x} \in \Omega \setminus \{\mathbf{x}_1, \ldots, \mathbf{x}_m\}\,; \qquad \partial_n V = 0\,, \quad \mathbf{x} \in \partial\Omega\,; \tag{2.8a}$$

$$V \sim A_j^v \log|\mathbf{x} - \mathbf{x}_j| + \frac{A_j^v}{\nu} + \frac{1}{d_1^v}(D_v A_j^v + d_2^v \eta_j)\,, \quad \text{as} \quad \mathbf{x} \to \mathbf{x}_j\,, \qquad j \in \{1, \ldots, m\}\,. \tag{2.8b}$$

To represent solutions to (2.7) and (2.8), we introduce the *reduced-wave* Green's function $G_\omega(\mathbf{x}, \mathbf{x}_j)$ that satisfies

$$\Delta G_\omega - \omega^2 G_\omega = -\delta(\mathbf{x} - \mathbf{x}_j)\,, \quad \mathbf{x} \in \Omega\,; \qquad \partial_n G_\omega = 0\,, \quad \mathbf{x} \in \partial\Omega\,; \tag{2.9a}$$

$$G_\omega \sim -\frac{1}{2\pi}\log|\mathbf{x} - \mathbf{x}_j| + R_\omega(\mathbf{x}_j) + o(1)\,, \quad \text{as} \quad \mathbf{x} \to \mathbf{x}_j\,. \tag{2.9b}$$

Here $R_\omega(\mathbf{x}_j)$ is the regular, or non-singular, part of the singularity at $\mathbf{x} = \mathbf{x}_j$. The solutions to (2.7) and (2.8) are represented as

$$U(\mathbf{x}) = -2\pi \sum_{i=1}^m A_i^u G_{\omega_u}(\mathbf{x}; \mathbf{x}_i)\,, \qquad V(\mathbf{x}) = -2\pi \sum_{i=1}^m A_i^v G_{\omega_v}(\mathbf{x}; \mathbf{x}_i)\,. \tag{2.10}$$

The pre-specification of the regular part of each singularity condition in (2.7) and (2.8) yields a constraint. These constraints provide algebraic systems for A_j^u and A_j^v for $j \in \{1, \ldots, m\}$. By expanding (2.10) as $\mathbf{x} \to \mathbf{x}_j$, we enforce that that the non-singular terms in the resulting expression agree with the conditions that are required in (2.7b) and (2.8b) for each $j \in \{1, \ldots, m\}$. This leads to linear algebraic systems for $\mathcal{A}^u \equiv (A_1^u, \ldots, A_m^u)^T$ and $\mathcal{A}^v \equiv (A_1^v, \ldots, A_m^v)^T$, given in matrix form by

$$\left(\left(1 + \frac{\nu D_u}{d_1^u}\right) I + 2\pi\nu\mathcal{G}_{\omega_u}\right)\mathcal{A}^u = -\frac{\nu d_2^u}{d_1^u}\,\mu\,, \qquad \left(\left(1 + \frac{\nu D_v}{d_1^v}\right) I + 2\pi\nu\mathcal{G}_{\omega_v}\right)\mathcal{A}^v = -\frac{\nu d_2^v}{d_1^v}\,\eta\,, \tag{2.11}$$

where $\mu \equiv (\mu_1, \ldots, \mu_m)^T$ and $\eta \equiv (\eta_1, \ldots, \eta_m)^T$. In (2.11), $\mathcal{G}_\omega$ with either $\omega = \omega_u$ or $\omega = \omega_v$ is the symmetric reduced-wave Greens' interaction matrix defined by

$$\mathcal{G}_\omega \equiv \begin{pmatrix} R_{\omega 1} & G_{\omega 12} & \ldots & G_{\omega 1m} \\ G_{\omega 21} & R_{\omega 2} & \ldots & G_{\omega 2m} \\ \vdots & \vdots & \ddots & \vdots \\ G_{\omega m1} & G_{\omega m2} & \ldots & R_{\omega m} \end{pmatrix}. \tag{2.12}$$

Here $G_{\omega ji} = G_{\omega ij} \equiv G_\omega(\mathbf{x}_j; \mathbf{x}_i)$ for $i \neq j$, and $R_{\omega j} \equiv R_\omega(\mathbf{x}_j)$ for $j \in \{1, \ldots, m\}$, are obtained from the solution to (2.9).

To determine a nonlinear algebraic system that characterizes our steady-state solution, we solve (2.11) for $\mathcal{A}^v$ and $\mathcal{A}^u$, and substitute the resulting expressions into (2.6). In this way, we obtain a $2m$ dimensional nonlinear algebraic system for μ_j and η_j, for $j = 1, \ldots, m$, given by

$$f(\mu_j, \eta_j) - \mathbf{e}_j^T \Theta_u \mu = 0\,, \qquad g(\mu_j, \eta_j) - \mathbf{e}_j^T \Theta_v \eta = 0\,, \quad \text{for} \quad j \in \{1, \ldots, m\}\,, \tag{2.13a}$$

where $\mathbf{e}_j \equiv (0, \ldots, 0, 1, 0, \ldots, 0)^T$ is the unit vector in the j^{th} direction. In (2.13a), Θ_u and Θ_v are defined by

$$\Theta_u \equiv 2\pi\nu D_u \frac{d_2^u}{d_1^u}\left[\left(1 + \frac{\nu D_u}{d_1^u}\right) I + 2\pi\nu\mathcal{G}_{\omega_u}\right]^{-1}, \qquad \Theta_v \equiv 2\pi\nu D_v \frac{d_2^v}{d_1^v}\left[\left(1 + \frac{\nu D_v}{d_1^v}\right) I + 2\pi\nu\mathcal{G}_{\omega_v}\right]^{-1}. \tag{2.13b}$$

We can simplify our steady-state analysis for the special case where $g(\mu, \eta)$ is linear and inhibiting in η, with the form

$$g(\mu, \eta) = g_1(\mu) - g_2\eta\,, \tag{2.14}$$

where $g_2 \geq 0$ is a constant. This specific form applies to Gierer-Meinhardt [15], Rauch-Millonas [49], and FitzHugh-Nagumo [17] reaction kinetics, and is relevant for the illustrations of the theory given in §4. In this case, we obtain from the second equation in (2.13a) that

$$\eta = [g_2 I + \Theta_v]^{-1}\,\mathbf{g}_1 \qquad \text{where} \qquad \mathbf{g}_1 \equiv (g_1(\mu_1), \ldots, g_1(\mu_m))^T\,. \tag{2.15}$$

Then, from the first equation in (2.13a) we obtain an m dimensional nonlinear algebraic system for $\mu = (\mu_1, \ldots, \mu_m)^T$ given by

$$f\left(\mu_j, \mathbf{e}_j^T (g_2 I + \Theta_v)^{-1} \mathbf{g}_1\right) - \mathbf{e}_j^T \Theta_u \mu = 0\,, \qquad j \in \{1, \ldots, m\}\,. \tag{2.16}$$

Next, we define a symmetric cell arrangement for which the steady-state analysis can be further simplified.

Definition 2.1. *A* **symmetric cell arrangement** *is defined by the condition that the symmetric Green's matrix $\mathcal{G}_\omega$ satisfies the following two properties:*

- **Property 1:** $\mathbf{e} \equiv (1, \ldots, 1)^T$ *is an eigenvector of $\mathcal{G}_\omega$ for all $\omega > 0$:*
- **Property 2:** *The eigenspace of $\mathcal{G}_\omega$ orthogonal to* $\mathbf{e}$ *is independent of ω.*

These two properties certainly hold when $\mathcal{G}_\omega$ is a circulant matrix. In particular, $\mathcal{G}_\omega$ is a circulant matrix when m small cells are equidistantly spaced on a ring that is concentric within a circular domain Ω. Such an arrangement of cells is called a **ring pattern**.

For a symmetric cell arrangement, $\mathcal{G}_{\omega_u}$ and $\mathcal{G}_{\omega_v}$ have a common eigenspace, and so we can seek a symmetric solution to (2.13) of the form

$$\mu = \mu_c \mathbf{e}\,, \quad \eta = \eta_c \mathbf{e}\,, \quad \mathcal{A}^u = A_c^u \mathbf{e}\,, \quad \mathcal{A}^v = A_c^v \mathbf{e}\,, \tag{2.17}$$

where the scalars μ_c, η_c, A_c^u, and A_c^v are to be found. Upon substituting (2.17) into (2.13), we obtain that μ_c and η_c satisfy the nonlinear algebraic system

$$f(\mu_c, \eta_c) - \alpha_u \mu_c = 0\,, \qquad g(\mu_c, \eta_c) - \alpha_v \eta_c = 0\,, \tag{2.18}$$

where α_u and α_v, denoting the eigenvalues of Θ_u and Θ_v for the eigenvector $\mathbf{e}$, respectively, are defined by

$$\alpha_u \equiv \frac{2\pi\nu D_u d_2^u/d_1^u}{1 + \nu D_u/d_1^u + 2\pi\nu\kappa_u}\,, \qquad \alpha_v \equiv \frac{2\pi\nu D_v d_2^v/d_1^v}{1 + \nu D_v/d_1^v + 2\pi\nu\kappa_v}\,. \tag{2.19a}$$

Here κ_u and κ_v are the eigenvalues of the Green's matrices for the eigenvector $\mathbf{e}$, given by

$$\mathcal{G}_{\omega_u}\mathbf{e} = \kappa_u \mathbf{e}\,, \qquad \mathcal{G}_{\omega_v}\mathbf{e} = \kappa_v \mathbf{e}\,. \tag{2.19b}$$

Moreover, if $g(\mu, \eta)$ has the specific form in (2.14), we obtain from (2.16) that for a symmetric pattern of cells, there is a symmetric steady-state solution whenever there is a root μ_c to the scalar nonlinear algebraic equation

$$f\left(\mu_c, \frac{g_1(\mu_c)}{g_2 + \alpha_v}\right) - \alpha_u \mu_c = 0\,. \tag{2.20}$$

In summary, for a symmetric pattern of cells, the asymptotic construction of a symmetric steady-state solution for (2.3) is reduced to the much simpler problem of determining a solution to the two-dimensional nonlinear algebraic problem (2.18) for general reaction kinetics, or to (2.20) when g has the specific form in (2.14). In these algebraic problems, the eigenvalues κ_u and κ_v, as needed in (2.19a), are the constant row sums of the Green's matrices for the two bulk species. The bulk diffusivities, the membrane reaction rates, and the spatial configuration of the cells all influence α_u and α_v.

2.3 Symmetry-breaking bifurcations

To detect any symmetry-breaking pitchfork bifurcation points along the symmetric steady-state solution branch we can perform a linear stability analysis of (2.3) around the steady-state solution and seek $\lambda = 0$ eigenvalue crossings. An equivalent, but simpler, approach to detect zero-eigenvalue crossings for the linearized problem is to determine bifurcation points associated with the linearization of the nonlinear algebraic system (2.13) around a symmetric steady-state.

To do so, we introduce the perturbations

$$\mu = \mu_c \mathbf{e} + \tilde{\mu}\,, \qquad \eta = \eta_c \mathbf{e} + \tilde{\eta}\,, \qquad \mathcal{A}^u = A_c^u \mathbf{e} + \tilde{\mathcal{A}}^u\,, \qquad \mathcal{A}^v = A_c^v \mathbf{e} + \tilde{\mathcal{A}}^v\,, \tag{2.21}$$

into (2.13) and linearize the resulting system. In this way, we obtain that a symmetry-breaking bifurcation occurs if and only if there is a non-trivial solution to the $2m \times 2m$ homogeneous linear system

$$\begin{pmatrix} f_\mu^c I - \Theta_u & f_\eta^c I \\ g_\mu^c I & g_\eta^c I - \Theta_v \end{pmatrix} \begin{pmatrix} \tilde{\mu} \\ \tilde{\eta} \end{pmatrix} = \begin{pmatrix} \mathbf{0} \\ \mathbf{0} \end{pmatrix}\,, \tag{2.22}$$

at some point along the symmetric solution branch given by (2.18). In (2.22) we have labeled f_μ^c by $f_\mu^c \equiv \partial_\mu f(\mu, \eta)$ when evaluated at $\mu = \mu_c$ and $\eta = \eta_c$, while I is the $m \times m$ identity matrix. For the special case where g has the specific form in (2.14), we can solve (2.22) for $\tilde{\eta}$ and reduce (2.22) to the m-dimensional homogeneous linear system

$$\left(f_\mu^c I + f_\eta^c g_1'(\mu_c) \left(g_2 I + \Theta_v \right)^{-1} - \Theta_u \right) \tilde{\mu} = \mathbf{0}\,. \tag{2.23}$$

Next, by Property 2 for a symmetric cell arrangement, it follows that $\mathcal{G}_{\omega_u}$ and $\mathcal{G}_{\omega_v}$ have a common orthogonal eigenspace $\mathcal{Q}^\perp \equiv \text{span}\{\mathbf{q}_2, \ldots, \mathbf{q}_m\}$, where $\mathbf{q}_j^T \mathbf{e} = 0$ for $j \in \{2, \ldots, m\}$ and $\mathbf{q}_i^T \mathbf{q}_j = 0$ for $i \neq j$. The eigenvalues of $\mathcal{G}_{\omega_u}$ and $\mathcal{G}_{\omega_v}$ in this common eigenspace are labeled by

$$\mathcal{G}_{\omega_u} \mathbf{q}_j = \kappa_{u,j}^\perp \mathbf{q}_j\,, \qquad \mathcal{G}_{\omega_v} \mathbf{q}_j = \kappa_{v,j}^\perp \mathbf{q}_j\,, \qquad j \in \{2, \ldots, m\}\,, \tag{2.24}$$

so that

$$\Theta_u \mathbf{q}_j = \alpha_{u,j}^\perp \mathbf{q}_j\,, \qquad \Theta_v \mathbf{q}_j = \alpha_{v,j}^\perp \mathbf{q}_j\,, \qquad j \in \{2, \ldots, m\}\,, \tag{2.25}$$

with

$$\alpha_{u,j}^\perp \equiv \frac{2\pi\nu D_u d_2^u / d_1^u}{1 + \nu D_u / d_1^u + 2\pi\nu\kappa_{u,j}^\perp}\,, \qquad \alpha_{v,j}^\perp \equiv \frac{2\pi\nu D_v d_2^v / d_1^v}{1 + \nu D_v / d_1^v + 2\pi\nu\kappa_{v,j}^\perp}\,. \tag{2.26}$$

By setting $\tilde{\mu} = \tilde{\mu}_c \mathbf{q}_j$ and $\tilde{\eta} = \tilde{\eta}_c \mathbf{q}_j$ in (2.22), we conclude that a symmetry-breaking bifurcation occurs for the j^{th} mode with $j \in \{2, \ldots, m\}$ whenever

$$\begin{pmatrix} f_\mu^c - \alpha_{u,j}^\perp & f_\eta^c \\ g_\mu^c & g_\eta^c - \alpha_{v,j}^\perp \end{pmatrix} \begin{pmatrix} \tilde{\mu}_c \\ \tilde{\eta}_c \end{pmatrix} = \begin{pmatrix} 0 \\ 0 \end{pmatrix}\,, \tag{2.27}$$

has a nontrivial solution. This is equivalent to the condition that

$$\left(f_\mu^c - \alpha_{u,j}^\perp \right) \left(g_\eta^c - \alpha_{v,j}^\perp \right) - f_\eta^c g_\mu^c = 0\,, \qquad j \in \{2, \ldots, m\}\,, \tag{2.28}$$

is satisfied at some point along the symmetric solution branch defined by the solution to (2.18).

Finally, for the special case where g has the specific form in (2.14), we obtain that there is a symmetry-breaking bifurcation for the j^{th} mode, with $j \in \{2, \ldots, m\}$, when there is a root to the scalar problem

$$f_\mu^c + \frac{f_\eta^c g_1'(\mu_c)}{g_2 + \alpha_{v,j}^\perp} - \alpha_{u,j}^\perp = 0\,, \tag{2.29}$$

whenever $\eta_c = g_1(\mu_c)/(g_2 + \alpha_v)$ where μ_c satisfies (2.20).

In the examples shown in §4 we will use $\rho \equiv d_1^v / d_1^u = d_2^v / d_2^u$ as the bifurcation parameter to detect whether symmetry-breaking bifurcations can occur along the symmetric solution branch.

2.4 A symmetric cell arrangement with two cells

Consider a symmetric cell arrangement with two cells, i.e. $m = 2$, for the special case where g has the form in (2.14). Then, to determine all steady-state solutions we need only solve the nonlinear algebraic system (2.16) for μ_1 and μ_2. The symmetric steady-state solution, for which $\mu_c \equiv \mu_1 = \mu_2$, is obtained by solving the scalar problem (2.20). To detect whether symmetry-breaking bifurcations can occur, we note that $\mathbf{q}_2 = (1, -1)^T$ spans the common eigenspace of $\mathcal{G}_{\omega_u}$ and $\mathcal{G}_{\omega_v}$ orthogonal to $\mathbf{e}$, and that $\kappa_u = R_{\omega_u 1} - G_{\omega_u 12}$ and $\kappa_v = R_{\omega_v 1} - G_{\omega_v 12}$ are the associated eigenvalues for $\mathbf{q}_2$. This yields that the root-finding condition (2.29) becomes

$$f^c_\mu + \frac{f^c_\eta g_1'(\mu_c)}{g_2 + \alpha^\perp_{v,2}} - \alpha^\perp_{u,2} = 0\,, \tag{2.30}$$

where in terms of the entries of the Green's matrices we have

$$\alpha^\perp_{u,2} \equiv \frac{2\pi\nu D_u d_2^u/d_1^u}{1 + \nu D_u/d_1^u + 2\pi\nu\,[R_{\omega_u 1} - G_{\omega_u 12}]}\,, \qquad \alpha^\perp_{v,2} \equiv \frac{2\pi\nu D_v d_2^v/d_1^v}{1 + \nu D_v/d_1^v + 2\pi\nu\,[R_{\omega_v 1} - G_{\omega_v 12}]}\,. \tag{2.31}$$

To detect any pitchfork bifurcation points on the symmetric steady-state branch parameterized by $\rho = d_1^v/d_1^u = d_2^v/d_2^u$ we numerically solve (2.20) together with (2.30). In §4 we illustrate this approach for certain reaction kinetics when Ω is the unit disk, where the reduced-wave Green's function is known analytically (see Appendix B).

3 The Linear Stability Analysis

In this section, we formulate the linear stability problem for the steady-state solutions constructed in §2.2. We denote the bulk steady-state solutions of §2.2 by $u_e(\mathbf{x})$ and $v_e(\mathbf{x})$, and the steady-state vector of intracellular steady-states by $\mu_e = (\mu_{e1}, \ldots, \mu_{em})^T$ and $\eta_e = (\eta_{e1}, \ldots, \eta_{em})^T$.

To formulate the linear stability problem, we first introduce the perturbations

$$\begin{aligned} &u(t,\mathbf{x}) = u_e(\mathbf{x}) + e^{\lambda t}\phi(\mathbf{x})\,, \qquad v(t,\mathbf{x}) = v_e(\mathbf{x}) + e^{\lambda t}\psi(\mathbf{x})\,, \\ &\mu_j(t) = \mu_{ej} + e^{\lambda t}\xi_j\,, \qquad \eta_j(t) = \eta_{ej} + e^{\lambda t}\zeta_j\,, \qquad \text{for} \quad j \in \{1, \ldots, m\}\,, \end{aligned}$$

into (2.3) and linearize the resulting system. This yields the eigenvalue problem

$$\text{bulk} \qquad \begin{cases} \Delta\phi - \Omega_u^2\phi = 0\,, & \mathbf{x} \in \Omega \backslash \bigcup_{j=1}^m \Omega_j\,, \\ \Delta\psi - \Omega_v^2\psi = 0\,, & \mathbf{x} \in \Omega \backslash \bigcup_{j=1}^m \Omega_j\,, \\ \partial_{\bar{n}}\phi = \partial_{\bar{n}}\psi = 0\,, & \mathbf{x} \in \partial\Omega\,, \end{cases} \tag{3.1a}$$

$$\text{reaction fluxes} \qquad \begin{cases} \varepsilon D_u \partial_{n_j}\phi = d_1^u\phi - d_2^u\xi_j\,, & \mathbf{x} \in \partial\Omega_j\,, \\ \varepsilon D_v \partial_{n_j}\psi = d_1^v\psi - d_2^v\zeta_j, & \mathbf{x} \in \partial\Omega_j\,, \end{cases} \tag{3.1b}$$

$$\text{compartments} \qquad \begin{cases} (\lambda I - J_j)\begin{pmatrix}\xi_j \\ \zeta_j\end{pmatrix} = \varepsilon^{-1}\begin{pmatrix}\int_{\partial\Omega_j}(d_1^u\phi - d_2^u\xi_j)\,dS \\ \int_{\partial\Omega_j}(d_1^v\psi - d_2^v\zeta_j)\,dS\end{pmatrix}\,, \qquad j \in \{1, \ldots, m\}\,. \end{cases} \tag{3.1c}$$

Here the Jacobian matrix J_j of the intracellular kinetics, as well as Ω_u and Ω_v are defined by

$$J_j \equiv \begin{pmatrix}\partial_\mu f(\mu,\eta) & \partial_\eta f(\mu,\eta) \\ \partial_\mu g(\mu,\eta) & \partial_\eta g(\mu,\eta)\end{pmatrix}\Big|_{\mu=\mu_{ej},\eta=\eta_{ej}}\,, \qquad \Omega_u \equiv \sqrt{\frac{\lambda+\sigma_u}{D_u}}\,, \qquad \Omega_v \equiv \sqrt{\frac{\lambda+\sigma_v}{D_v}}\,. \tag{3.2}$$

We now use strong localized perturbation theory [60] to analyze (3.1) in the limit $\varepsilon \to 0$. In this way we will derive a nonlinear matrix eigenvalue problem, referred to as the globally coupled eigenvalue problem (GCEP), for the discrete eigenvalues λ of the linearization. This GCEP will be used to investigate various instabilities of the steady-state solutions constructed in §2.2.

In the $\mathcal{O}(\varepsilon)$ inner region near the j^{th} cell we introduce the local variables $\mathbf{y}_j = \varepsilon^{-1}(\mathbf{x} - \mathbf{x}_j)$, $\phi_j(\mathbf{x}) \equiv \phi(\mathbf{x}_j + \varepsilon\mathbf{y}_j)$ and $\psi_j(\mathbf{x}) \equiv \psi(\mathbf{x}_j + \varepsilon\mathbf{y}_j)$, with $p_j = |\mathbf{y}_j|$. Upon writing (3.1a) in terms of the inner variables, for $\varepsilon \to 0$ we

obtain in the j^{th} inner region that $\Delta\phi_j = 0$ and $\Delta\psi_j = 0$, for $p_j \geq 1$, subject to $D_u\,\partial_{p_j}\phi_j = d_1^u\phi_j - d_2^u\xi_j$ and $D_v\,\partial_{p_j}\psi_j = d_1^v\psi_j - d_2^v\zeta_j$ on $p_j = 1$. The radially symmetric solutions to these problems are

$$\phi_j(p_j) = c_j^u \log p_j + \frac{1}{d_1^u}\left(D_u\, c_j^u + d_2^u\xi_j\right)\,, \qquad \psi_j(p_j) = c_j^v \log p_j + \frac{1}{d_1^v}\left(D_v\, c_j^v + d_2^v\zeta_j\right)\,, \tag{3.3}$$

for $j \in \{1,\dots,m\}$, where c_j^u and c_j^v for $j \in \{1,\dots,m\}$ are constants to be determined. Upon substituting (3.3) into (3.1c) we obtain, in terms of the Jacobian J_j of (3.2), that

$$(\lambda I - J_j)\begin{pmatrix}\xi_j\\ \zeta_j\end{pmatrix} = \begin{pmatrix}2\pi D_u c_j^u\\ 2\pi D_v c_j^v\end{pmatrix}\,, \qquad \text{for} \quad j \in \{1,\dots,m\}\,. \tag{3.4}$$

To determine c_j^u and c_j^v we must match the far-field behavior of the inner solutions (3.3) to the outer solutions defined in the bulk region. Similar to the analysis of the steady-state solution, we obtain that

$$\Delta\phi - \Omega_u^2\,\phi = 0\,, \quad \mathbf{x} \in \Omega \setminus \{\mathbf{x}_1,\dots,\mathbf{x}_m\}\,; \qquad \partial_n\phi = 0\,, \quad \mathbf{x} \in \partial\Omega\,; \tag{3.5a}$$

$$U \sim c_j^u \log|\mathbf{x}-\mathbf{x}_j| + \frac{c_j^u}{\nu} + \frac{1}{d_1^u}(D_u c_j^u + d_2^u\xi_j)\,, \quad \text{as} \quad \mathbf{x} \to \mathbf{x}_j\,, \qquad j \in \{1,\dots,m\}\,, \tag{3.5b}$$

where $\nu \equiv -1/\log\varepsilon \ll 1$. Similarly, for the perturbation of the other bulk species we obtain

$$\Delta\psi - \Omega_v^2\,\psi = 0\,, \quad \mathbf{x} \in \Omega \setminus \{\mathbf{x}_1,\dots,\mathbf{x}_m\}\,; \qquad \partial_n\psi = 0\,, \quad \mathbf{x} \in \partial\Omega\,; \tag{3.6a}$$

$$\psi \sim c_j^v \log|\mathbf{x}-\mathbf{x}_j| + \frac{c_j^v}{\nu} + \frac{1}{d_1^v}(D_v c_j^v + d_2^v\zeta_j)\,, \quad \text{as} \quad \mathbf{x} \to \mathbf{x}_j\,, \qquad j \in \{1,\dots,m\}\,. \tag{3.6b}$$

The solutions to (3.5) and (3.6) are represented as

$$\phi(x) = -2\pi\sum_{i=1}^m c_i^u G_{u,\lambda}(\mathbf{x};\mathbf{x}_i)\,, \qquad \psi(x) = -2\pi\sum_{i=1}^m c_i^v G_{v,\lambda}(\mathbf{x};\mathbf{x}_i)\,, \tag{3.7}$$

where, to simplify the notation and emphasize the dependence on the eigenvalue parameter λ, we have defined

$$G_{u,\lambda}(\mathbf{x};\mathbf{x}_j) \equiv G_{\Omega_u}(\mathbf{x};\mathbf{x}_j)\,, \qquad G_{v,\lambda}(\mathbf{x};\mathbf{x}_j) \equiv G_{\Omega_v}(\mathbf{x};\mathbf{x}_j)\,, \tag{3.8}$$

where $G_\omega(\mathbf{x};\mathbf{x}_j)$ is defined by the solution to (2.9). Upon letting $\mathbf{x} \to \mathbf{x}_j$ in (3.7) and ensuring that the singularity conditions in (3.5b) and (3.6b) are satisfied, we obtain a linear algebraic system for the vectors $\mathbf{c}^u \equiv (c_1^u,\dots,c_m^u)^T$ and $\mathbf{c}^v \equiv (c_1^v,\dots,c_m^v)^T$, given in matrix form by

$$\left(\left(1+\frac{\nu D_u}{d_1^u}\right)I + 2\pi\nu\mathcal{G}_{u,\lambda}\right)\mathbf{c}^u = -\frac{\nu d_2^u}{d_1^u}\,\xi\,, \qquad \left(\left(1+\frac{\nu D_v}{d_1^v}\right)I + 2\pi\nu\mathcal{G}_{v,\lambda}\right)\mathbf{c}^v = -\frac{\nu d_2^v}{d_1^v}\,\zeta\,, \tag{3.9}$$

where $\xi \equiv (\xi_1,\dots,\xi_m)^T$ and $\zeta \equiv (\zeta_1,\dots,\zeta_m)^T$. In (3.9), $\mathcal{G}_{u,\lambda}$ and $\mathcal{G}_{v,\lambda}$ denote the reduced-wave Green's matrix given in (2.12) with either $\omega = \Omega_u$ or $\omega = \Omega_v$, respectively. Here Ω_u and Ω_v are defined in terms of λ by (3.2).

Assuming that λ is not an eigenvalue of J_j for any $j \in \{1,\dots,m\}$, we obtain upon inverting (3.4) and writing the system in matrix form that

$$\xi = 2\pi D_u \mathrm{K}_{11}\mathbf{c}^u + 2\pi D_v \mathrm{K}_{12}\mathbf{c}^v\,, \qquad \zeta = 2\pi D_u \mathrm{K}_{21}\mathbf{c}^u + 2\pi D_v \mathrm{K}_{22}\mathbf{c}^v\,, \tag{3.10}$$

where $\xi = (\xi_1,\dots,\xi_m)^T$ and $\zeta = (\zeta_1,\dots,\zeta_m)^T$. Here K_{11}, K_{12}, K_{21}, and K_{22} are the diagonal matrices defined by

$$\mathrm{K}_{11} \equiv \mathrm{diag}(K_{11j})\,, \qquad \mathrm{K}_{12} \equiv \mathrm{diag}(K_{12j})\,, \qquad \mathrm{K}_{21} \equiv \mathrm{diag}(K_{21j})\,, \qquad \mathrm{K}_{22} \equiv \mathrm{diag}(K_{22j})\,, \tag{3.11a}$$

with diagonal entries given by

$$K_{11j} \equiv \mathbf{e}_1^T(\lambda I - J_j)^{-1}\mathbf{e}_1\,, \quad K_{12j} \equiv \mathbf{e}_1^T(\lambda I - J_j)^{-1}\mathbf{e}_2\,, \quad K_{21j} \equiv \mathbf{e}_2^T(\lambda I - J_j)^{-1}\mathbf{e}_1\,, \quad K_{22j} \equiv \mathbf{e}_2^T(\lambda I - J_j)^{-1}\mathbf{e}_2\,, \tag{3.11b}$$

where $\mathbf{e}_1 = (1,0)^T$ and $\mathbf{e}_2 = (0,1)^T$.

Then, upon substituting (3.9) into (3.10), we obtain the $2m \times 2m$ homogeneous algebraic system, which we write in block matrix form as

$$\mathcal{M}(\lambda)\begin{pmatrix}\mathbf{c}^u\\ \mathbf{c}^v\end{pmatrix} = \begin{pmatrix}\mathbf{0}\\ \mathbf{0}\end{pmatrix}, \qquad \text{where} \qquad \mathcal{M}(\lambda) \equiv \begin{pmatrix}\mathcal{M}_u(\lambda) & \mathcal{H}_u(\lambda)\\ \mathcal{M}_v(\lambda) & \mathcal{H}_v(\lambda)\end{pmatrix}, \tag{3.12a}$$

with

$$\mathcal{M}_u(\lambda) \equiv \left(1 + \frac{\nu D_u}{d_1^u}\right) I + 2\pi\nu D_u \frac{d_2^u}{d_1^u}\mathrm{K}_{11} + 2\pi\nu\mathcal{G}_{u,\lambda}\,, \qquad \mathcal{H}_u(\lambda) \equiv 2\pi\nu D_v \frac{d_2^u}{d_1^u}\mathrm{K}_{12}\,, \tag{3.12b}$$

$$\mathcal{H}_v(\lambda) \equiv 2\pi\nu D_u \frac{d_2^v}{d_1^v}\mathrm{K}_{21}\,, \qquad \mathcal{M}_v(\lambda) \equiv \left(1 + \frac{\nu D_v}{d_1^v}\right) I + 2\pi\nu D_v \frac{d_2^v}{d_1^v}\mathrm{K}_{22} + 2\pi\nu\mathcal{G}_{v,\lambda}\,. \tag{3.12c}$$

The nonlinear matrix eigenvalue problem (3.12) is referred to as the globally coupled eigenvalue problem (GCEP). The GCEP has a nontrivial solution $(\mathbf{c}^u, \mathbf{c}^v)^T \neq (\mathbf{0},\mathbf{0})^T$, if and only λ satisfies $\det \mathcal{M}(\lambda) = 0$. The set $\Lambda(\mathcal{M})$, defined by

$$\Lambda(\mathcal{M}) \equiv \{\lambda \,|\, \det \mathcal{M}(\lambda) = 0\}\,, \tag{3.13}$$

is the union of all such roots. Any element $\lambda \in \Lambda(\mathcal{M})$ satisfying $\mathrm{Re}(\lambda) > 0$ provides an approximation, valid as $\varepsilon \to 0$, for an unstable discrete eigenvalue of the linearized problem (3.1). However, if for all $\lambda \in \Lambda(\mathcal{M})$ we have $\mathrm{Re}(\lambda) < 0$, then the steady-state solution is linearly stable.

When there is a large number of cells m, the determination of the discrete eigenvalues comprising $\Lambda(\mathcal{M})$ is in general a very challenging numerical problem. A survey of nonlinear matrix eigenvalue problems and available solution strategies that apply to only certain classes of matrices is given in [22] and [3]. Specific applications of nonlinear matrix problems in simpler contexts where $\mathcal{M}(\lambda)$ is either a polynomial or a rational function of λ are discussed in [2]. Since for our problem, $\mathcal{M}(\lambda)$ is not symmetric and has a complicated dependence on the eigenvalue parameter through the Green's matrices and from the diagonal K matrices of (3.11), these previously developed numerical strategies are not applicable for computing the set $\Lambda(\mathcal{M})$ in (3.13) for a steady-state solution with an arbitrary collection of cells.

For a symmetric steady-state solution corresponding to a symmetric cell arrangement, we now verify that the condition $\det(\mathcal{M}(0)) = 0$ in (3.12) is equivalent to the zero-eigenvalue crossing condition derived in (2.22), which was based on a linearization of the nonlinear algebraic system around the symmetric steady-state. When $\lambda = 0$, we have

$$2\pi D_u \mathbf{c}^u = -\Theta_u \xi\,, \qquad 2\pi D_v \mathbf{c}^v = -\Theta_v \zeta\,,$$

where Θ_u and Θ_v are defined in (2.13b). Since K_{11}, K_{12}, K_{22}, and K_{21} are all multiples of the identity for a symmetric steady-state, we obtain from (3.12) together with (3.9) that when $\lambda = 0$ we have in block matrix form

$$\begin{pmatrix}\xi\\ \zeta\end{pmatrix} + \begin{pmatrix}K_{11}I & K_{12}I\\ K_{12}I & K_{22}I\end{pmatrix}\begin{pmatrix}\Theta_u & 0\\ 0 & \Theta_v\end{pmatrix}\begin{pmatrix}\xi\\ \zeta\end{pmatrix} = \begin{pmatrix}\mathbf{0}\\ \mathbf{0}\end{pmatrix}. \tag{3.14}$$

Here we have re-defined the scalars K_{11}, K_{12}, K_{21}, and K_{22} by $\mathrm{K}_{11} = K_{11}I$, $\mathrm{K}_{12} = K_{12}I$, $\mathrm{K}_{21} = K_{21}I$, and $\mathrm{K}_{22} = K_{22}I$. When $\lambda = 0$, we calculate that

$$\mathcal{K} = \begin{pmatrix}K_{11}I & K_{12}I\\ K_{21}I & K_{22}I\end{pmatrix} = -J_c^{-1}, \quad \text{where} \quad J_c \equiv \begin{pmatrix}f_\mu^c I & f_\eta^c I\\ g_\mu^c I & g_\eta^c I\end{pmatrix}.$$

Finally, upon multiplying (3.14) by J_c, and using $J_c\mathcal{K} = -I$, we readily obtain that

$$\begin{pmatrix}f_\mu^c I - \Theta_u & f_\eta^c I\\ g_\mu^c I & g_\eta^c I - \Theta_v\end{pmatrix}\begin{pmatrix}\xi\\ \zeta\end{pmatrix} = \begin{pmatrix}\mathbf{0}\\ \mathbf{0}\end{pmatrix}, \tag{3.15}$$

which is precisely the same as in (2.22).

3.1 Re-formulation of the linear stability problem

A simpler formulation of the linear stability problem that applies to both symmetric and asymmetric steady-state solutions can be done when g has the specific form in (2.14). In this situation, we can write (3.4) in the form

$$\zeta_j = \frac{g_1'(\mu_j)}{\lambda + g_2}\xi_j + \frac{2\pi D_v}{\lambda + g_2}c_j^v\,, \qquad (\lambda - f_\mu(\mu_j,\eta_j))\,\xi_j - f_\eta(\mu_j,\eta_j)\zeta_j = 2\pi D_u c_j^u\,.$$

Then, upon relating c_j^v and c_j^u to ζ_j and ξ_j by using (3.9), we obtain in matrix form that

$$\zeta = \frac{1}{\lambda + g_2}\Lambda_2\xi - \frac{1}{\lambda + g_2}\Theta_{v,\lambda}\zeta\,, \qquad \Lambda_3\xi - \Lambda_4\zeta = -\Theta_{u,\lambda}\xi\,, \tag{3.16}$$

where $\Theta_{u,\lambda}$, $\Theta_{v,\lambda}$, and the diagonal matrices Λ_2, Λ_3, and Λ_4 are defined by

$$\Theta_{u,\lambda} \equiv 2\pi\nu D_u\frac{d_2^u}{d_1^u}\left[\left(1 + \frac{\nu D_u}{d_1^u}\right)I + 2\pi\nu\mathcal{G}_{u,\lambda}\right]^{-1}\,, \quad \Theta_{v,\lambda} \equiv 2\pi\nu D_v\frac{d_2^v}{d_1^v}\left[\left(1 + \frac{\nu D_v}{d_1^v}\right)I + 2\pi\nu\mathcal{G}_{v,\lambda}\right]^{-1} \tag{3.17a}$$

$$\Lambda_2 \equiv \mathrm{diag}(g_1'(\mu_j))\,, \qquad \Lambda_3 \equiv \mathrm{diag}(\lambda - f_\mu(\mu_j,\eta_j))\,, \qquad \Lambda_4 \equiv \mathrm{diag}(f_\eta(\mu_j,\eta_j))\,. \tag{3.17b}$$

Upon eliminating ζ in (3.16), we obtain the following nonlinear eigenvalue problem for the case where g has the form in (2.14):

$$\mathcal{N}(\lambda)\xi = \mathbf{0}\,, \qquad \text{where} \qquad \mathcal{N}(\lambda) \equiv \Lambda_3 - \Lambda_4\left[(\lambda + g_2)I + \Theta_{v,\lambda}\right]^{-1}\Lambda_2 + \Theta_{u,\lambda}\,. \tag{3.18}$$

Observe that setting $\det(\mathcal{N}(\lambda)) = 0$ involves root-finding on the determinant of a matrix of size $m \times m$ rather than that for the larger $2m \times 2m$ matrix, as needed for (3.13).

The characterization (3.18) is particularly useful for determining the linear stability properties of a symmetric steady-state for a symmetric cell arrangement when g has the form in (2.14). For a symmetric steady-state with $\lambda = 0$, we obtain from (3.17) that $\Lambda_2 = g_1'(\mu_c)I$, $\Lambda_3 = -f_\mu^c I$, and $\Lambda_4 = f_\eta^c I$. From (3.18), this yields that

$$\mathcal{N}(0) = -f_\mu^c I - f_\eta^c g_1'(\mu_c)\left[g_2 I + \Theta_{v,0}\right]^{-1} + \Theta_{u,0}\,.$$

Since $\Theta_{u,\lambda} = \Theta_u$ and $\Theta_{v,\lambda} = \Theta_v$ when $\lambda = 0$, where Θ_u and Θ_v were defined in (2.13b), we obtain that the condition $\det(\mathcal{N}(0)) = 0$ is equivalent to the formulation (2.23) derived in §2.3, which was based on linearizing the nonlinear algebraic system around the symmetric steady-state solution.

For a symmetric steady-state solution of a symmetric cell arrangement, one key advantage of the re-formulation (3.18) is that the discrete eigenvalues of the linearization (3.1) can be determined by finding the union of the roots of m scalar problems. This is done by using $\det(\mathcal{N}(\lambda)) = \prod_{j=1}^m \sigma_j(\lambda)$, where $\sigma_j(\lambda)$ for $j = \{1,\ldots,m\}$ are the eigenvalues of $\mathcal{N}(\lambda)$. More specifically, since $\mathcal{G}_{u,\lambda}$ and $\mathcal{G}_{v,\lambda}$ have the common eigenspace

$$\mathcal{G}_{u,\lambda}\mathbf{e} = \kappa_{u,\lambda}\mathbf{e}\,, \quad \mathcal{G}_{v,\lambda}\mathbf{e} = \kappa_{v,\lambda}\mathbf{e}\,; \qquad \mathcal{G}_{u,\lambda}\mathbf{q}_j = \kappa_{u,\lambda j}^{\perp}\mathbf{q}_j\,, \quad \mathcal{G}_{v,\lambda}\mathbf{q}_j = \kappa_{v,\lambda j}^{\perp}\mathbf{q}_j\,, \qquad j \in \{2,\ldots,m\}\,, \tag{3.19a}$$

the eigenvalue $\sigma_1(\lambda)$ corresponding to $\mathbf{e}$ and the eigenvalues $\sigma_j(\lambda)$ corresponding to $\mathbf{q}_j$, for $j \in \{2,\ldots,m\}$ are readily calculated. A simple calculation yields that

$$\sigma_1(\lambda) = \lambda - f_\mu^c - \frac{f_\eta^c g_1'(\mu_c)}{\lambda + g_2 + \alpha_{v,\lambda}} + \alpha_{u,\lambda}\,, \tag{3.20a}$$

$$\sigma_j(\lambda) = \lambda - f_\mu^c - \frac{f_\eta^c g_1'(\mu_c)}{\lambda + g_2 + \alpha_{v,\lambda j}^{\perp}} + \alpha_{u,\lambda j}^{\perp}\,, \qquad j \in \{2,\ldots,m\}\,, \tag{3.20b}$$

where we have defined

$$\alpha_{u,\lambda} \equiv \frac{2\pi\nu D_u d_2^u/d_1^u}{1 + \nu D_u/d_1^u + 2\pi\nu\kappa_{u,\lambda}}\,, \qquad \alpha_{v,\lambda} \equiv \frac{2\pi\nu D_v d_2^v/d_1^v}{1 + \nu D_v/d_1^v + 2\pi\nu\kappa_{v,\lambda}}\,, \tag{3.20c}$$

$$\alpha_{u,\lambda j}^{\perp} \equiv \frac{2\pi\nu D_u d_2^u/d_1^u}{1 + \nu D_u/d_1^u + 2\pi\nu\kappa_{u,\lambda j}^{\perp}}\,, \qquad \alpha_{v,\lambda j}^{\perp} \equiv \frac{2\pi\nu D_v d_2^v/d_1^v}{1 + \nu D_v/d_1^v + 2\pi\nu\kappa_{v,\lambda j}^{\perp}}\,, \qquad j \in \{2,\ldots,m\}\,. \tag{3.20d}$$

With this re-formulation, for a symmetric steady-state of a symmetric cell arrangement, and with g of the form in (2.14), the set of discrete eigenvalues of the linearization, $\Lambda(\mathcal{M})$, in (3.13) can be written conveniently as

$$\Lambda(\mathcal{M}) \equiv \{\lambda \,|\, \sigma_1(\lambda) = 0\} \;\cup\; \bigcup_{j=2}^{m} \{\lambda \,|\sigma_j(\lambda) = 0\}\,. \tag{3.21}$$

In summary, to determine the linear stability properties of this symmetric steady-state solution we need only solve m scalar root-finding problems and determine whether there are any roots in $\mathrm{Re}(\lambda) > 0$. This is considerably more tractable numerically than performing a root-finding based on the determinant of the GCEP in (3.18).

4 Illustrations of the theory: A ring pattern of cells

In this section we illustrate the steady-state and linear stability theory developed in §2.2 and §3 for a ring pattern of cells inside unit disk Ω, for which the Green's function is given analytically in Appendix B. We will show that symmetry-breaking bifurcations can occur for the Gierer-Meinhardt [15], Rauch-Millonas [49] and FitzHugh-Nagumo [17] reaction kinetics. The theoretical prediction of stable asymmetric patterns will be confirmed through full time-dependent numerical simulations of (2.3) computed using FlexPDE [13].

For a ring pattern of m cells in the unit disk with ring radius r, with $0 < r < 1$, the cell centers are located at

$$\mathbf{x}_k = r\left(\cos\left(\frac{2\pi(k-1)}{m}\right), \sin\left(\frac{2\pi(k-1)}{m}\right)\right), \qquad k \in \{1,\ldots,m\}\,. \tag{4.1}$$

For a ring pattern of cells, all Green matrices are symmetric and circulant and have the common eigenspace

$$\mathbf{v}_k = (1, Z_k, Z_k^2, ..., Z_k^{m-1})^T \quad \text{with} \quad Z_k \equiv \exp\left(\frac{2\pi i(k-1)}{m}\right) \quad \text{and} \quad k \in \{1, ..., m\}\,,$$

which are a basis of $\mathbb{C}^m$. In (B.2) of Appendix B we summarize how to obtain the matrix spectrum of a symmetric and circulant matrix that has a real-valued basis for the eigenspace.

In our illustrations of the theory below, we will assume for simplicity that the membrane reaction rates satisfy

$$d_1^u = d_2^u \equiv d_u \qquad d_1^v = d_2^v \equiv d_v\,, \qquad \text{with} \quad \rho \equiv \frac{d_v}{d_u}\,, \tag{4.2}$$

and that $g(\mu,\eta)$ has the specific form in (2.14). We will focus on a two-cell ring pattern in the unit disk, as shown schematically in Figure 2, for three specific reaction kinetics.

To numerically implement our asymptotic theory, the steady-state solution branches are computed from (2.16) with $m = 2$ using the parameter continuation software MatCont [7], while the symmetric solution branch is obtained from (2.20). Symmetry-breaking bifurcation points in ρ along the symmetric branch are identified by numerically solving (2.30) together with (2.20). Finally, to determine the linear stability properties of the symmetric branch we need only determine if there exists a λ with $\mathrm{Re}(\lambda) > 0$ in the set $\Lambda(\mathcal{M})$ given in (3.21). For $m = 2$, this is done by calculating all the roots of $\sigma_1(\lambda) = 0$ and $\sigma_2(\lambda) = 0$ by using (3.20) and the explicit expressions for the eigenvalues of the Green's matrices as can be obtained from Appendix B.

4.1 Gierer-Meinhardt reaction kinetics

We consider a prototypical Gierer-Meinhardt model (GM), where the nonlinear reaction kinetics are confined within the compartments. The original GM model, introduced in [15] and [14] to model pattern formation in biological morphogenesis, has the form

$$\partial_t u = D_u\Delta u - \sigma_u u + \varrho_0(x) + c_u\varrho_u(x)\frac{u^2}{v}\,, \qquad \partial_t v = D_v\Delta v - \sigma_v v + c_v\varrho_v(x)u^2\,.$$

This model disregards that in biological tissues morphogen-producing reactions mostly occur intracellularly and on the membranes of cells. For simplicity, we illustrate our compartmental-reaction diffusion theory for the specific

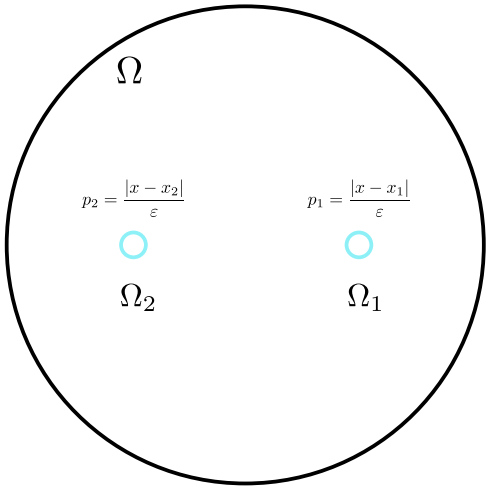

Figure 2: A schematic plot of a ring pattern in the unit disk with two cells. The bifurcation parameter for symmetry-breaking is ρ, while the diffusivities satisfy $D_u = D_v$.

case where $\varrho_0 \equiv 0, c_u\varrho_u(x) \equiv 1$, and $c_v\varrho_v \equiv 1$. When there is no bulk diffusion, the compartments are uncoupled from the bulk and we impose the intracellular reaction kinetics

$$\dot{\mu}(t) = f(\mu,\eta) \equiv \frac{\mu^2}{\eta}\,, \qquad \dot{\eta}(t) = g(\mu,\eta) \equiv \mu^2\,. \tag{4.3}$$

The uncoupled equilibrium for (4.3) given by $\mu_e = 0$, and where η_e is an arbitrary constant, is non-hyberbolic in all directions.

To apply the bulk-cell steady-state analysis of §2 for a two-cell ring pattern, we first identify that $g(\mu,\eta) = g_1(\mu) - g_2\eta$, where $g_1 = \mu^2$ and $g_2 = 0$. For $m = 2$, we conclude from (2.16) that all steady-states of the bulk-cell system are associated with the nonlinear algebraic problem

$$\begin{aligned} f(\mu_{e1}, \mathbf{e}_1^T\Theta_v^{-1}((\mu_{e1})^2,(\mu_{e2})^2)^T) - \mathbf{e}_1^T\Theta_u(\mu_{e1},\mu_{e2})^T &= 0 \\ f(\mu_{e2}, \mathbf{e}_2^T\Theta_v^{-1}((\mu_{e1})^2,(\mu_{e2})^2)^T) - \mathbf{e}_2^T\Theta_u(\mu_{e1},\mu_{e2})^T &= 0\,. \end{aligned} \tag{4.4}$$

The symmetric equilibrium (μ_e,η_e), which satisfies (2.20), is readily calculated as

$$\mu_e = \frac{\alpha_v}{\alpha_u}\,, \qquad \eta_e = \frac{\alpha_v}{\alpha_u^2}\,, \tag{4.5}$$

where α_u and α_v are defined in (2.19). By combining (4.5) with (2.30), we conclude that a symmetry-breaking bifurcation from the symmetric steady-state occurs whenever the condition

$$\frac{\alpha_v}{\alpha_{v,2}^{\perp}} + \frac{\alpha_{u,2}^{\perp}}{2\alpha_u} - 1 = 0\,, \tag{4.6}$$

is satisfied at some point along the symmetric solution branch. Here $\alpha_{u,2}^{\perp}$ and $\alpha_{v,2}^{\perp}$ were defined in (2.31).

In the left panel of Figure 3 we plot the bifurcation diagram of solutions to (4.4) for a parameter set where $D_v = D_u$ and with the other parameter values as in the figure caption. We observe that a supercritical symmetry-breaking pitchfork bifurcation from the symmetric branch occurs at the critical value $\rho = \rho_p \approx 9.79168$. In Figure 4 we show full PDE results for (2.3) computed with FlexPDE [13] for values of ρ on either side of this theoretically predicted bifurcation value. In the left panels of this figure, we observe that when $\rho = 5 < \rho_p$, an initial perturbation of the symmetric steady-state converges back to the symmetric steady-state as time increases. In contrast, when $\rho = 15 > \rho_p$, we observe from the right panels of Figure 4 that, for an initial condition near the symmetric steady-state, the time-dependent PDE solution converges as time increases to the asymmetric steady-state predicted in the left panel of Figure 3.

In the right panel of Figure 3 we show that the pitchfork bifurcation value for the emergence of asymmetric steady-states increases substantially when the ring radius for the two-cell pattern increases. As a result, we conclude that for cells that are farther apart, a larger value of ρ is needed to create a stable asymmetric pattern.

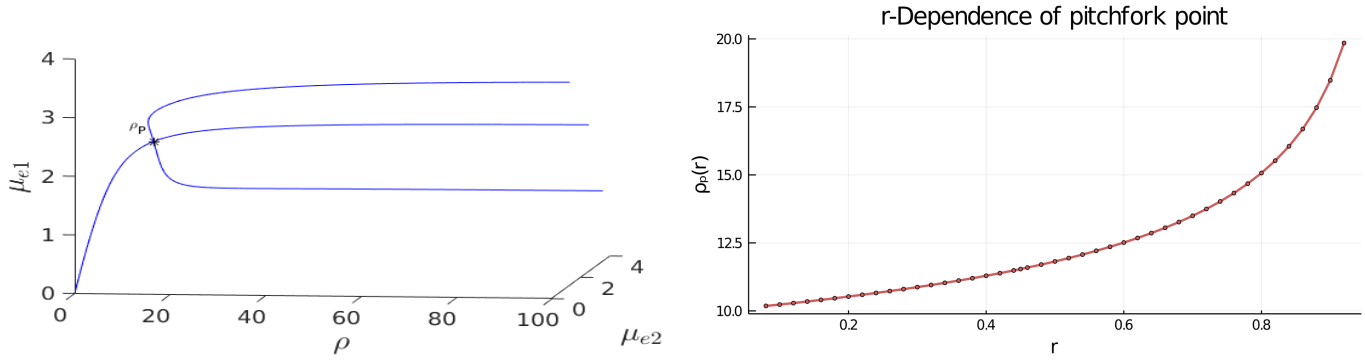

Figure 3: Left: 3-D Bifurcation diagram, computed from (4.4), showing symmetric and asymmetric steady-states of a two-cell ring pattern with ring radius $r = 0.5$ and GM kinetics (4.3). Asymmetric steady-states emerge at the supercritical pitchfork bifurcation point $\rho = \rho_p \approx 9.79168$ along the symmetric branch. Right: The pitchfork bifurcation value of ρ increases rapidly as the ring radius r, and consequently the distance between the cells, increases. The dots are the values computed from (4.6), while the curve is the interpolation by the plotting function in Julia [4]. Parameters: $D_u = D_v = 5, \sigma_u = \sigma_v = 0.6, d_u = 0.09$, and $\varepsilon = 0.03$.

We now show that by varying the membrane reaction rate d_u, which necessarily varies the membrane reaction rate to the v-species according to $d_v = \rho\, d_u$, the steady-state solution branches with GM kinetics (4.3) computed from (4.4) can exhibit a hysteresis structure for low d_u. The numerical results of Figure 5 show such a hysteretic bifurcation structure between the asymmetric and symmetric solution branches for two values of d_u. We observe that as d_u decreases the extent of the hysteresis increases. The range where hysteresis occurs is given by the separation $\rho_p - \rho_s$ between the pitchfork point ρ_p and the secondary fold bifurcation point ρ_s along each asymmetric branch. Numerical results for this range for a parameter set where hysteresis occurs when $d_u < 0.09$ is given in Table 1.

d_u	0.05	0.06	0.07	0.08	0.09	0.1	0.11	0.12	0.13	0.135
ρ_p	7.70971	7.66508	11.42015	8.62258	9.79168	11.81838	15.65552	24.82347	70.62460	> 1000 or $\nexists$
μ_e	2.78094	2.54938	3.21380	2.28060	2.19994	2.14061	2.09668	2.06422	2.04050	
ρ_s	6.27944	6.93251	6.82631	8.60260	-	-	-	-	-	-
μ_{e1}	3.27136	3.09001	3.45845	2.56189	-	-	-	-	-	-
μ_{e2}	1.12375	1.34489	0.87895	1.93057	-	-	-	-	-	-

Table 1: Numerical values (rounded to 5th decimal place) of the subcritical (or supercritical) pitchfork bifurcation point ρ_p, the fold bifurcation point ρ_s, and the associated values for the symmetric μ_e and one of the asymmetric (μ_{e1}, μ_{e2}) solution branches. As d_u increases from 0.05, the range of ρ where hysteresis occurs decreases, until a supercritical pitchfork bifurcation occurs when $d_u \approx 0.85$. Parameters: $D_u = D_v = 5, \sigma_u = \sigma_v = 0.6, \varepsilon = 0.03, r = 0.5$.

For the parameter set with $d_u = 0.05$, which corresponds to the bifurcation diagram shown in the right panel of Figure 5, the full time-dependent computations of (2.3) with FlexPDE [13], as shown in Figure 8, illustrate that for an initial condition near the symmetric steady-state branch, and with ρ either satisfying $\rho < \rho_s$ or $\rho_s < \rho < \rho_p$, the time-dependent solution converges to the stable symmetric steady-state solution. However, as shown in the left panel of Figure 9, for an initial condition near the asymmetric branch when ρ is in the hysteresis region $\rho_s < \rho < \rho_p$, the time-dependent solution converges to the asymmetric steady-state. Moreover, if $\rho > \rho_p$, the right panel of Figure 9 shows that for an initial condition near the unstable symmetric steady-state the time-dependent solution converges to the asymmetric steady-state solution.

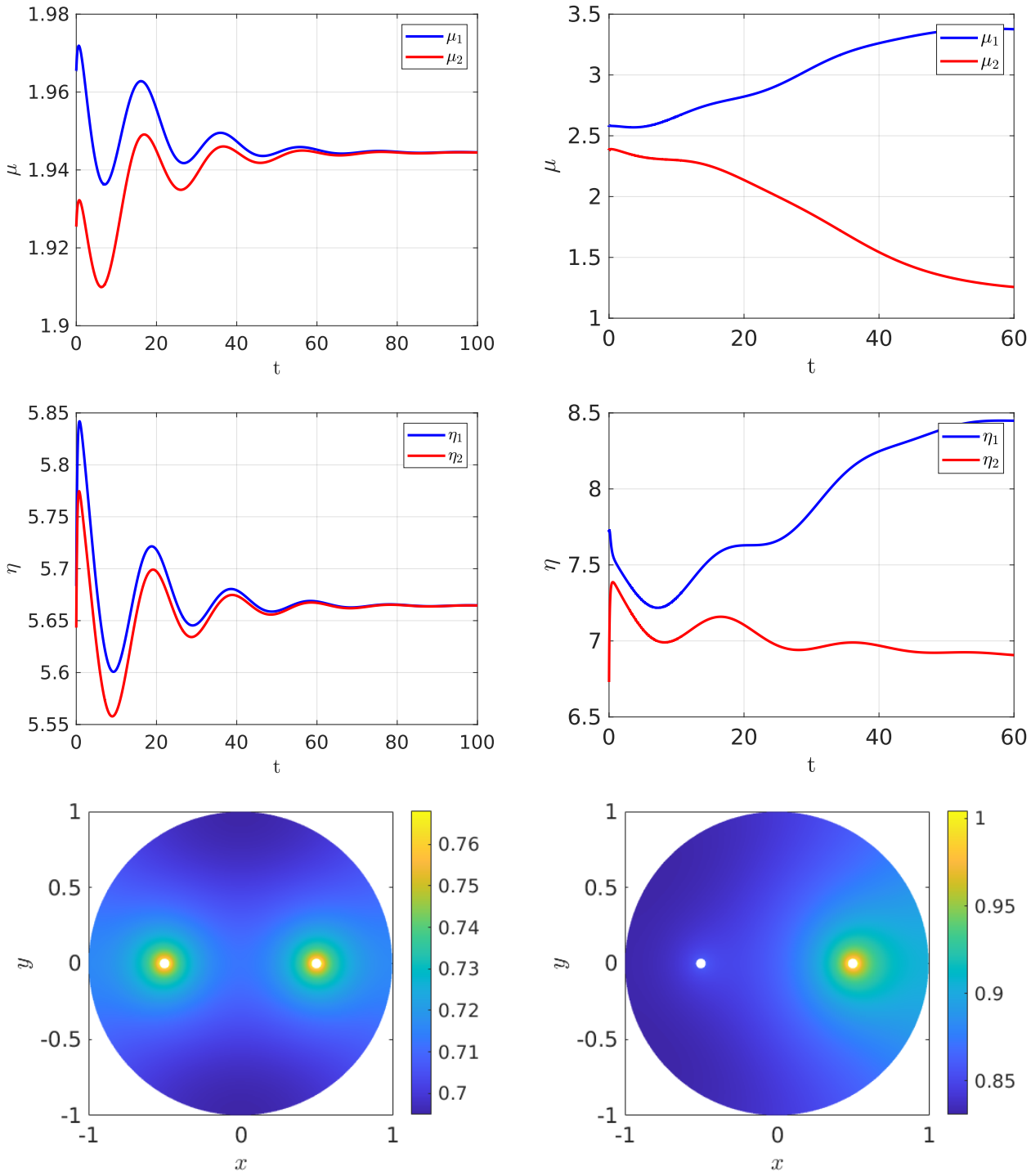

Figure 4: Full numerical PDE simulation results of (2.3) with FlexPDE [13] for GM kinetics (4.3). Left: convergence to the symmetric branch for $\rho = 5$ before the supercritical pitchfork point $\rho_p = 9.79168$, for an initial condition close to the symmetric branch. Right: convergence to the asymmetric branch selected by the eigenperturbation direction $\mathbf{q}_2 = (1, -1)^T$ for $\rho = 15$ and starting near the symmetric branch. Parameters: $D_u = D_v = 5, \sigma_u = \sigma_v = 0.6, d_u = 0.09, \varepsilon = 0.03$, and $r = 0.5$.

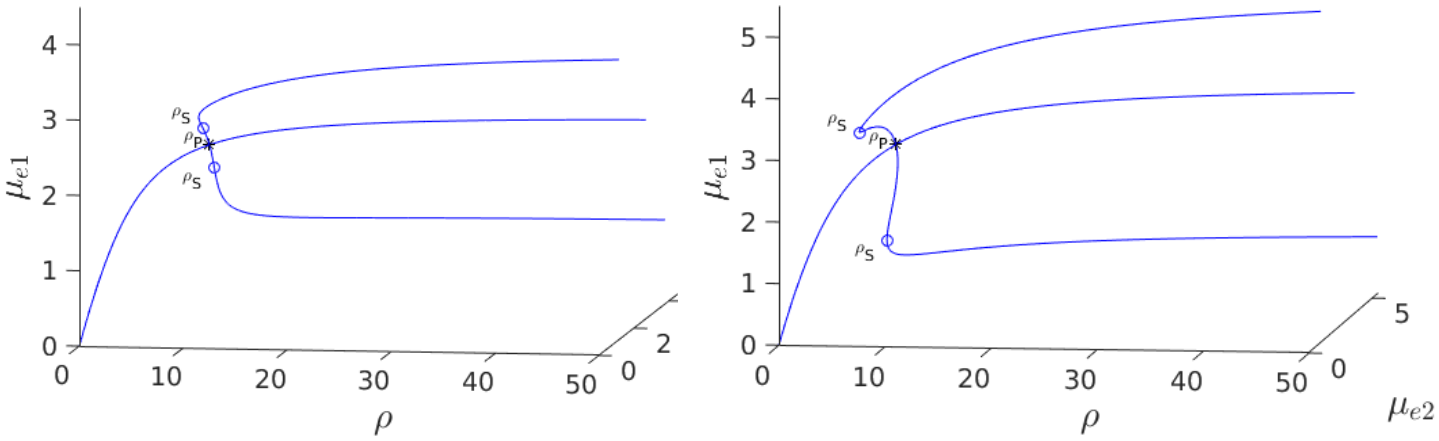

Figure 5: 3-D Bifurcation diagram, computed from (4.4), for symmetric and asymmetric steady-states of a two-cell ring pattern with ring radius $r = 0.5$ and two different values of d_u with GM kinetics (4.3). Left panel: $d_u = 0.08$. Right panel: $d_u = 0.05$. For these values of d_u, the steady-states exhibit hysteresis, i.e., a subcritical pitchfork bifurcation occurs from the symmetric equilibrium branch, with the emerging unstable asymmetric equilibrium branches regaining stability at a secondary fold point. Observe that the extent of the hysteresis increases when d_u decreases. Parameters: $D_u = D_v = 5, \sigma_u = \sigma_v = 0.6, \varepsilon = 0.03$, and $r = 0.5$.

To determine the linear stability properties of the symmetric steady-state solution branch as ρ is varied in Figures 3 and 5 we must determine the eigenvalues λ in the set (3.21). This is done by numerically computing the largest roots to $\sigma_1(\lambda) = 0$ and to $\sigma_2(\lambda) = 0$, as defined in (3.20). In Figure 6 we plot these roots versus ρ for two values of d_u. From this figure, we observe that in-phase perturbations of the symmetric steady-state solution branch, as determined by the roots of $\sigma_1(\lambda) = 0$, are always linearly stable. In contrast, anti-phase perturbations of the symmetric steady-state, as characterized by the roots of $\sigma_2(\lambda) = 0$, are linearly stable only for $\rho < \rho_p$, where ρ_p is the symmetry-breaking threshold. For $\rho > \rho_p$, the symmetric steady-state solution branch is unstable to an anti-phase eigenperturbation $\mathbf{q}_2 = (1, -1)^T$.

Next, to study the linear stability properties of the asymmetric steady-state solution branches we must determine whether the root-finding condition $\det(\mathcal{N}(\lambda)) = 0$ in (3.18) yields an eigenvalue with $\mathrm{Re}\lambda > 0$. The numerical results shown in Figure 7 for $d_u = 0.05$ (corresponding to the right panel in Figure 5), establishes that the asymmetric branch on the subcritical range $\rho_s < \rho < \rho_p$, which emanates from the symmetric steady-state branch, is unstable. However, as observed from Figure 7, the upper portion of the asymmetric branch for $\rho > \rho_s$ is linearly stable.

We now explore how the pitchfork bifurcation point depends on decreasing values of the diffusion coefficient ratio D_v/D_u when $d_u = 0.09$. When this ratio is unity, there was no hysteresis between the symmetric and asymmetric steady-state solution branches (see Table 1). We remark that a similar numerical experiment was performed in §2.3 of [45] for a 1-D compartmental-reaction diffusion model with GM kinetics with dynamically reactive boundaries. In our 2-D setting, we observe from the numerical results in Table 2 that a symmetry-breaking bifurcation can occur on the range $D_v/D_u < 1$, but only up until some minimum diffusion ratio threshold at which the pitchfork bifurcation point given by the root of (4.6) no longer exists. In addition, we observe that reducing the diffusion ratio threshold D_v/D_u below unity for fixed $d_u = 0.09$ does not introduce new hysteresis behavior, and the symmetry-breaking bifurcation remains supercritical.

Next, we set $d_u = 0.08$ where hysteresis occurs when $D_v/D_u = 1$, and we vary this diffusion ratio to determine whether hysteresis can be eliminated. Our numerical results in Figure 10 and Table 3 indicates that varying D_v/D_u does not eliminate the hysteresis between the symmetric and asymmetric steady-state branches. However, the extent of the hysteresis decreases as the ratio D_v/D_u increases.

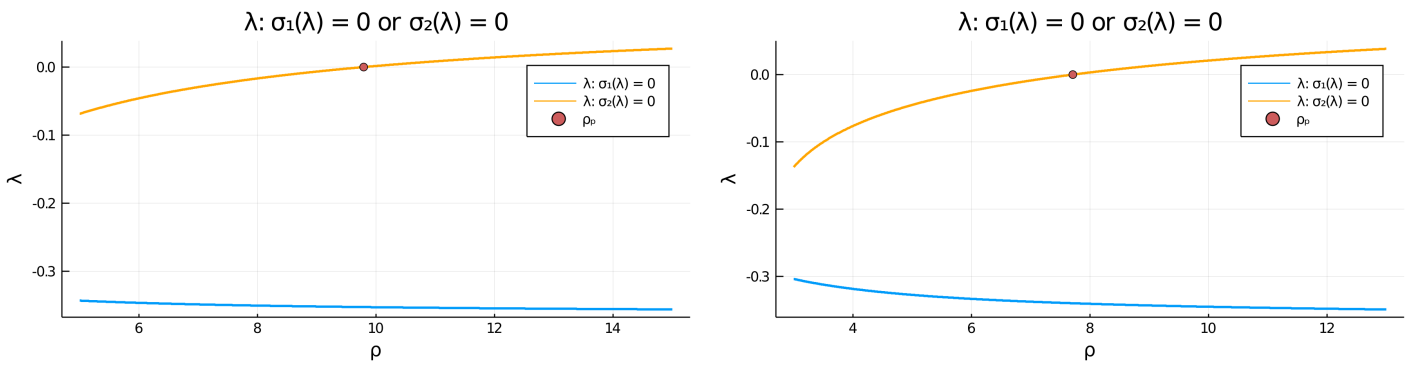

Figure 6: Plots of the numerically computed largest roots of $\sigma_1(\lambda) = 0$ and $\sigma_2(\lambda) = 0$ versus ρ, as defined in (3.20), that determine the linear stability properties to either in-phase $\mathbf{e} = (1, 1)^T$ or anti-phase $\mathbf{q}_2 = (1, -1)^T$ eigenperturbations of the symmetric steady-state solution, respectively. Left panel: for $d_u = 0.09$ we have $\rho_p \approx 9.79168$. Right panel: for $d_u = 0.05$ we have $\rho_p \approx 7.70971$. Observe that in-phase eigenperturbations are always linearly stable, whereas anti-phase eigenperturbations are linearly stable only on the range $\rho < \rho_p$ before the pitchfork point ρ_p. Parameters: $D_u = D_v = 5, \sigma_u = \sigma_v = 0.6, \varepsilon = 0.03, r = 0.5$.

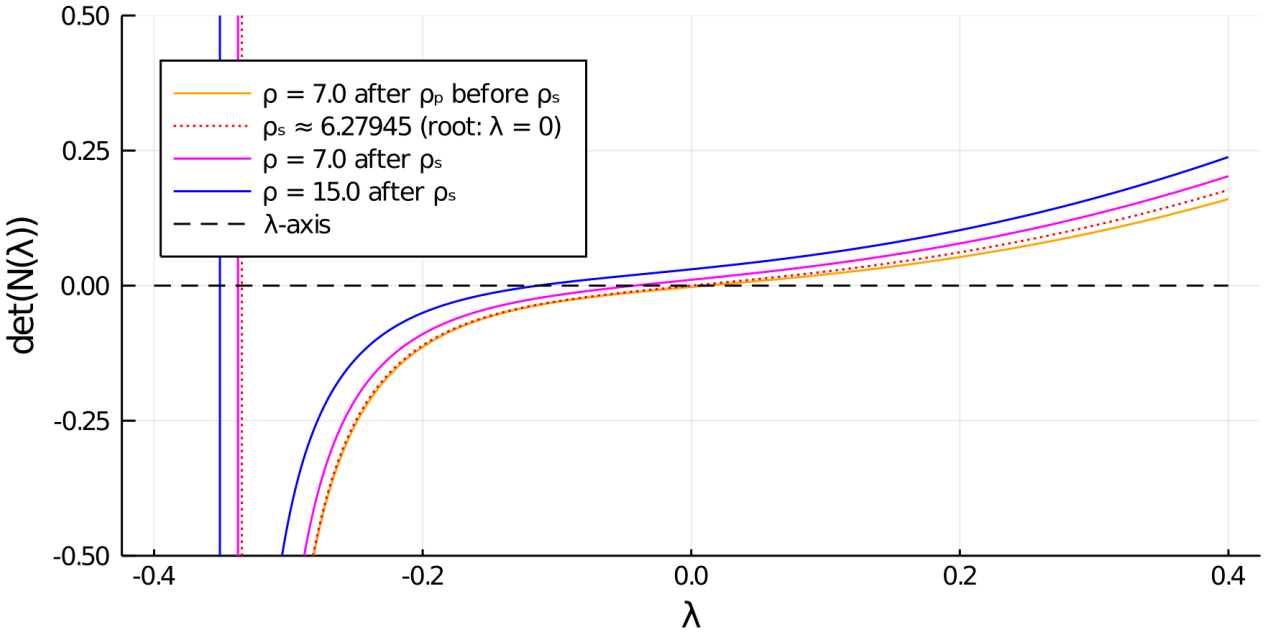

Figure 7: Zero-crossings of $\det(\mathcal{N}(\lambda)) = 0$, as defined in (3.18), determine the linear stability properties of an asymmetric steady-state solution with two cells. On the range $\rho_p < \rho < \rho_s$, before the secondary fold point along the asymmetric branch, we observe that $\lambda > 0$. This implies that the subcritical portion of the asymmetric steady-state branch between the pitchfork point and the fold point is unstable. Further along past the fold point the asymmetric branch regains stability. Parameters: $D_u = D_v = 5, \sigma_u = \sigma_v = 0.6, d_u = 0.05, \varepsilon = 0.03, r = 0.5$.

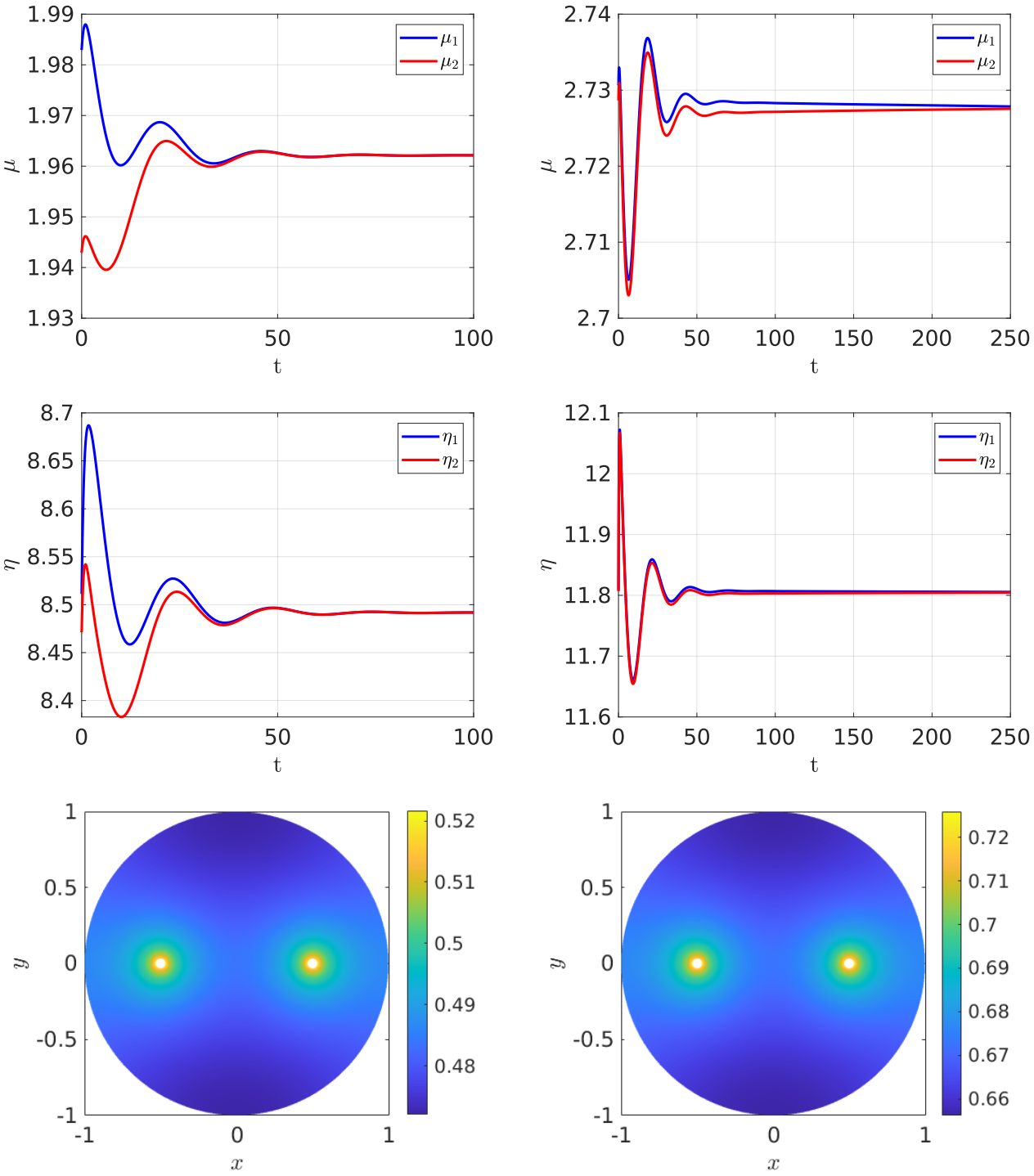

Figure 8: Full numerical simulation results of (2.3) with FlexPDE [13] for GM kinetics (4.3). Left: for an initial condition near the symmetric branch we observe convergence to the symmetric branch when $\rho = 4$, which is before the hysteresis region bounded by the fold point $\rho_s \approx 6.27945$ and the subcritical pitchfork point $\rho_p \approx 7.70971$. Right: convergence to the symmetric branch for $\rho = 7.2$, which lies on the range $\rho_s < \rho < \rho_p$, when starting near the symmetric branch. Parameters: $D_u = D_v = 5, \sigma_u = \sigma_v = 0.6, d_u = 0.05, \varepsilon = 0.03, r = 0.5$.

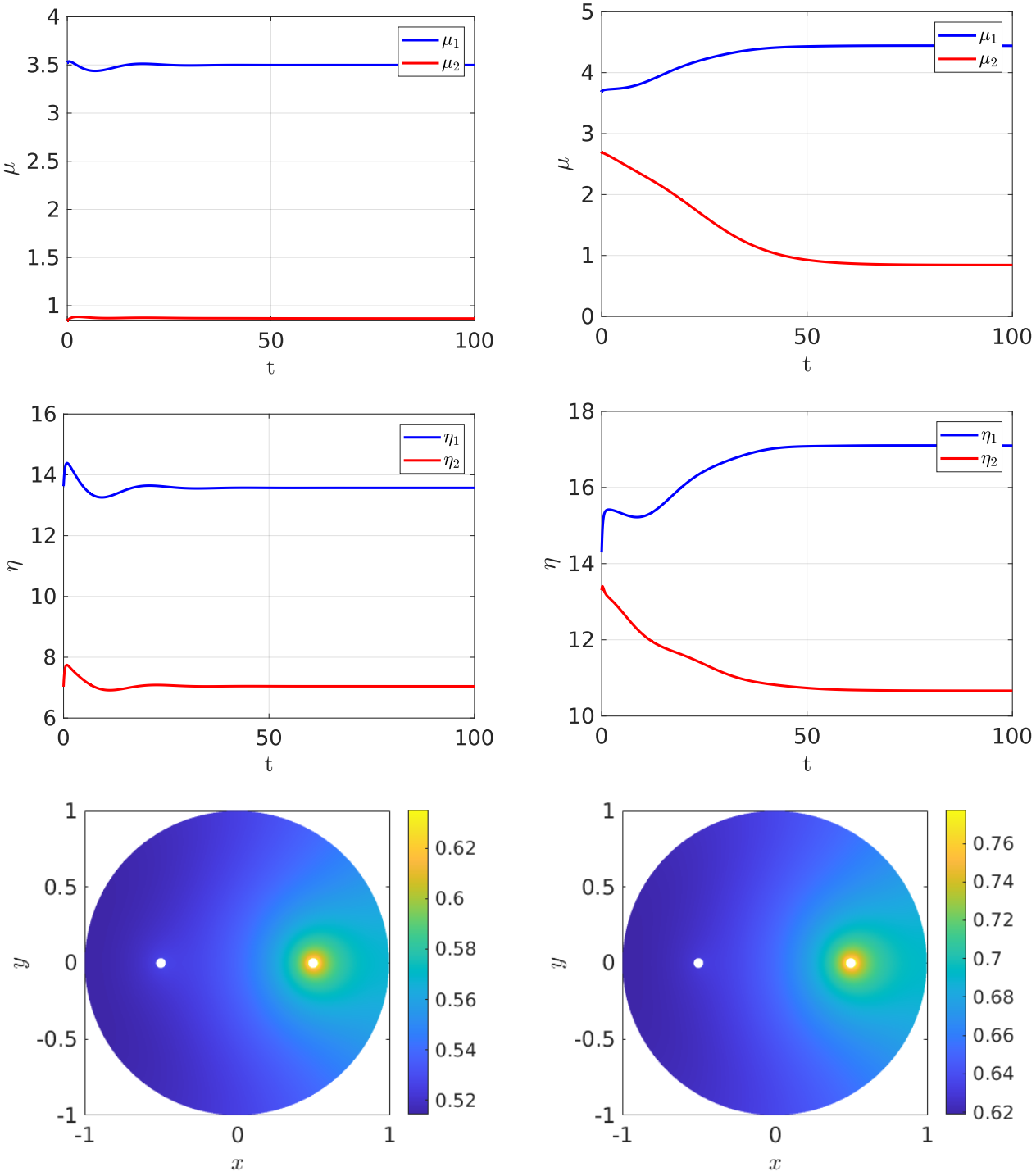

Figure 9: Full numerical simulation results of (2.3) with FlexPDE [13] for GM kinetics (4.3). Left: convergence to the asymmetric branch for an initial condition near this branch when $\rho = 7.2$ lies in the hysteresis region between the fold point $\rho_s \approx 6.27945$ and the subcritical pitchfork point $\rho_p \approx 7.70971$. Right: convergence to an asymmetric steady-state as selected by a small initial perturbation of the symmetric solution in the direction $\mathbf{q}_2 = (1, -1)$ when $\rho = 15 > \rho_p$. Parameters: $D_u = D_v = 5, \sigma_u = \sigma_v = 0.6, d_u = 0.05, \varepsilon = 0.03$, and $r = 0.5$.

D_v/D_u	0.42	0.43	0.5	0.6	0.8	1	1.2	1.4
ρ_p	> 1000 or ∄	573.56743	38.45836	19.56926	12.06861	9.79168	8.69082	8.04185
μ_e		2.32310	2.29271	2.26170	2.22305	2.19994	2.18456	2.17360
ρ_f	-	-	-	-	-	-	-	-
μ_{e1}	-	-	-	-	-	-	-	-
μ_{e2}	-	-	-	-	-	-	-	-

Table 2: Decreasing the ratio D_v/D_u does not trigger hysteresis when $d_u = 0.09$, but rather there is a minimum threshold of the diffusivity ratio where the symmetry-breaking pitchfork bifurcation point exists. The numerical values for the pitchfork point (ρ_p, μ_e) on the symmetric steady-state branch are again rounded to the 5th decimal place. Parameters: $D_u = 5, \sigma_u = \sigma_v = 0.6, d_u = 0.09, \varepsilon = 0.03, r = 0.5$.

D_v/D_u	0.37	0.38	0.4	0.6	0.8	1	3	5	8
ρ_p	> 1000 or ∄	197.98732	72.56533	14.30013	10.14347	8.62258	6.13144	5.79198	5.61640
μ_e		2.43797	2.42519	2.34462	2.30457	2.28061	2.21699	2.20432	2.19719
ρ_f		188.58078	71.25577	14.24676	10.11612	8.60260	6.12105	5.78264	5.60759
μ_{e1}		2.7386611	2.72431	2.63380	2.58881	2.56189	2.49043	2.47619	2.46819
μ_{e2}		2.063782	2.05297	1.98476	1.95085	1.93057	1.87672	1.86599	1.85996

Table 3: Increasing the diffusivity ratio D_v/D_u when $d_u = 0.08$ does not eliminate hysteresis, as the symmetry-breaking bifurcation point remains subcritical. The numerical values for the pitchfork point (ρ_p, μ_e) on the symmetric equilibrium branch and for one of the fold points $(\rho_s, \mu_{e1}, \mu_{e2})$ on the asymmetric branch are again rounded to the 5th decimal place. Parameters: $D_u = 5, \sigma_u = \sigma_v = 0.6, d_u = 0.08, \varepsilon = 0.03, r = 0.5$.

To obtain some analytical insight into the disappearance of the pitchfork point as shown in Tables 2 and 3 when the diffusivity ratio D_v/D_u decreases below a threshold, in Figure 11 we plot the function $F_\alpha(\rho) \equiv \alpha_v/\alpha_{v,2}^{\perp} + \alpha_{u,2}^{\perp}/(2\alpha_u) - 1$ versus ρ, representing the left-hand side of the pitchfork bifurcation condition (4.6), for several values of D_v/D_u, and for either $d_u = 0.08$ (left panel) or $d_u = 0.09$ (right panel). From (4.6) a root of $F_\alpha(\rho) = 0$ corresponds to a symmetry-breaking bifurcation point along the symmetric solution branch. From Figure 11 we observe that the asymptote of $F_\alpha(\rho)$ as $\rho \to \infty$ is positive when D_v/D_u is below a threshold, which eliminates the possibility of a pitchfork bifurcation point.

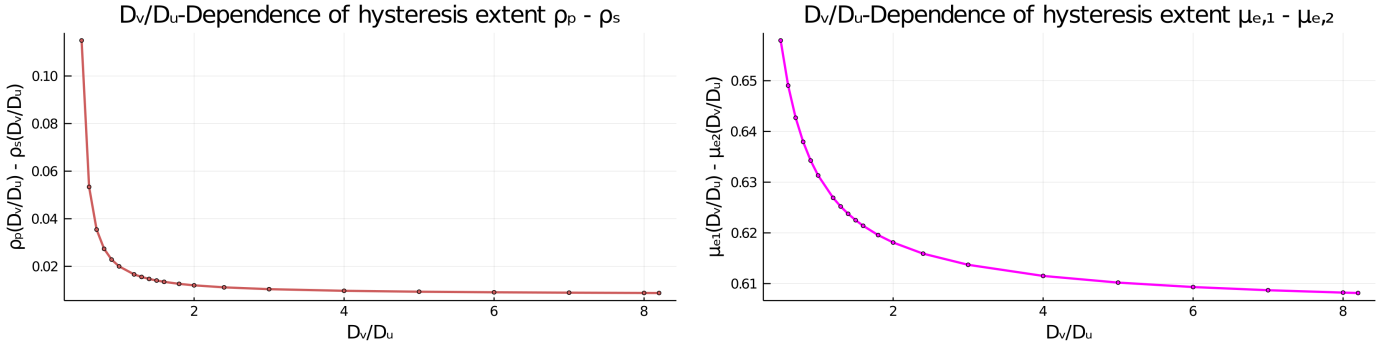

Figure 10: Effect of the diffusivity ratio D_v/D_u of the two bulk species on the extent of the hysteresis when $d_u = 0.08$, as measured by the distance between the fold bifurcation points and the subcritical pitchfork bifurcation point (left) and by the distance of the two asymmetric equilibria μ_{e1} and μ_{e2} from each other (right). The diffusivity $D_u = 5$ is fixed and the remaining parameters are as in Table 3. The dots are the numerically computed values using MatCont [7] that are interpolated by the plotting function in Julia [4].

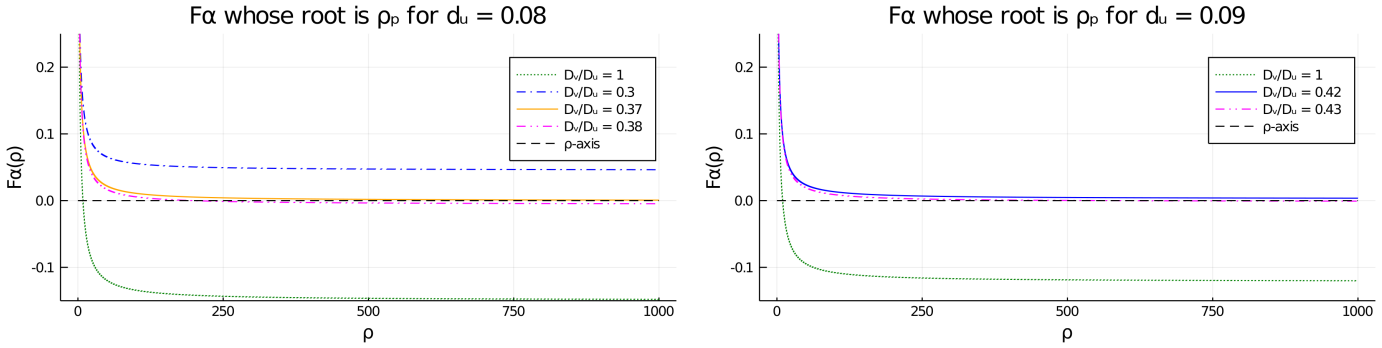

Figure 11: Effect of the diffusivity ratio D_v/D_u on the existence of the pitchfork point when $d_u = 0.08$ (left) and $d_u = 0.09$ (right). The numerical results show that the asymptote of $F_\alpha(\rho) \equiv \alpha_v/\alpha_{v,2}^\perp + \alpha_{u,2}^\perp/(2\alpha_u) - 1$ is positive for smaller values of D_v/D_u, as suggested by Tables 2 and 3. Therefore, when D_v/D_u falls below a threshold, the pitchfork bifurcation condition $F_\alpha(\rho) = 0$, which is equivalent to (4.6), no longer holds for any $\rho > 0$.

4.2 Rauch-Millonas reaction kinetics

Next, we consider the activator-inhibitor system proposed in [49] to universally model two-species signal transduction reaction kinetics between cells. This Rauch-Millonas (RM) intracellular kinetics of [49] is given by

$$\begin{aligned} \dot{\mu} &= c_u - q_u\mu + \frac{a_1^u\mu}{b_1^u+\mu} - \frac{a_2^u\mu\eta}{b_2^u+\mu} \equiv f(\mu,\eta) \\ \dot{\eta} &= c_v + w_v\mu - q_v\eta \equiv g(\mu,\eta)\,. \end{aligned} \tag{4.7}$$

Since g has the form in (2.14), we identify that $g_1(\mu) = c_v + w_v\mu$ and $g_2 = q_v$. We will choose a parameter set for which the reaction kinetics when uncoupled from the bulk has a unique linearly stable steady-state.

From (2.16), all steady-states of the bulk-cell model for a two-cell ring pattern are associated with the nonlinear algebraic system

$$\begin{aligned} f(\mu_{e1}, \mathbf{e}_1^T\left(q_vI + \Theta_v\right)^{-1}\left(c_v + w_v\mu_{e1}, c_v + w_v\mu_{e2}\right)^T) - \mathbf{e}_1^T\Theta_u(\mu_{e1},\mu_{e2})^T &= 0 \\ f(\mu_{e2}, \mathbf{e}_2^T\left(q_vI + \Theta_v\right)^{-1}\left(c_v + w_v\mu_{e1}, c_v + w_v\mu_{e2}\right)^T) - \mathbf{e}_2^T\Theta_u(\mu_{e1},\mu_{e2})^T &= 0\,. \end{aligned} \tag{4.8}$$

From (2.20), the symmetric steady-state solution branch is obtained from the solution μ_e to

$$c_u - q_u\mu_e + \frac{a_1^u\mu_e}{b_1^u+\mu_e} - \frac{a_2^u\mu_e}{b_2^u+\mu_e}\frac{(c_v + w_v\mu_e)}{q_v+\alpha_v} - \alpha_u\mu_e = 0\,, \tag{4.9}$$

where α_u and α_v are given in (2.19). Symmetry-breaking bifurcation points are obtained by solving the zero-eigenvalue crossing condition (2.30) together with (4.9). By solving for $w_v = w_v(\mu_e)$ in (2.30), we calculate

$$w_v(\mu_e) = \frac{-q_u + \frac{a_1^u}{b_1^u+\mu_e} - \frac{a_1^u\mu_e}{(b_1^u+\mu_e)^2} - \frac{a_2^u}{b_2^u+\mu_e}\frac{c_v}{q_v+\alpha_v} + \frac{a_2^u\mu_e}{(b_2^u+\mu_e)^2}\frac{c_v}{q_v+\alpha_v} - \alpha_{u,2}^\perp}{\frac{a_2^u}{b_2^u+\mu_e}\frac{\mu_e}{q_v+\alpha_v} - \frac{a_2^u\mu_e}{(b_2^u+\mu_e)^2}\frac{\mu_e}{q_v+\alpha_v} + \frac{a_2^u\mu_e}{b_2^u+\mu_e}\frac{1}{q_v+\alpha_{v,2}^\perp}}\,, \tag{4.10}$$

where $\alpha_{u,2}^\perp$ and $\alpha_{v,2}^\perp$ are defined in (2.31). By using (4.10) to eliminate ω_v in (4.9) we obtain a nonlinear algebraic equation that determines any symmetry-breaking bifurcation value for μ_e along the symmetric solution branch. The corresponding bifurcation value for w_v is obtained from (4.10).

For the parameter set given in the figure caption, we show in the left panel of Figure 12 that, for the fixed value $\rho = 15$, there is a degenerate w_v-pitchfork bubble, which is characterized by the emergence of asymmetric steady-state solutions at two values of w_v. From the right panel of Figure 12 we observe that in terms of ρ, and at a fixed w_v, the symmetry-breaking bifurcation is supercritical in ρ. For the parameter set in the right panel of Figure 12, we observe from Figure 13 that the eigenvalue λ determined by the root-finding condition $\sigma_2(\lambda) = 0$, with σ_2 given in (3.20), crosses through zero at the ρ-pitchfork bifurcation point along the symmetric steady-state branch. As a result, when $w_v = w_v^{P,2} \approx 7.08723$, the symmetric steady-state solution is linearly stable for $\rho < \rho_p = 15$, and is unstable on the range $\rho > \rho_p = 15$ to eigenperturbations in the direction of $\mathbf{q}_2 = (1,-1)^T$.

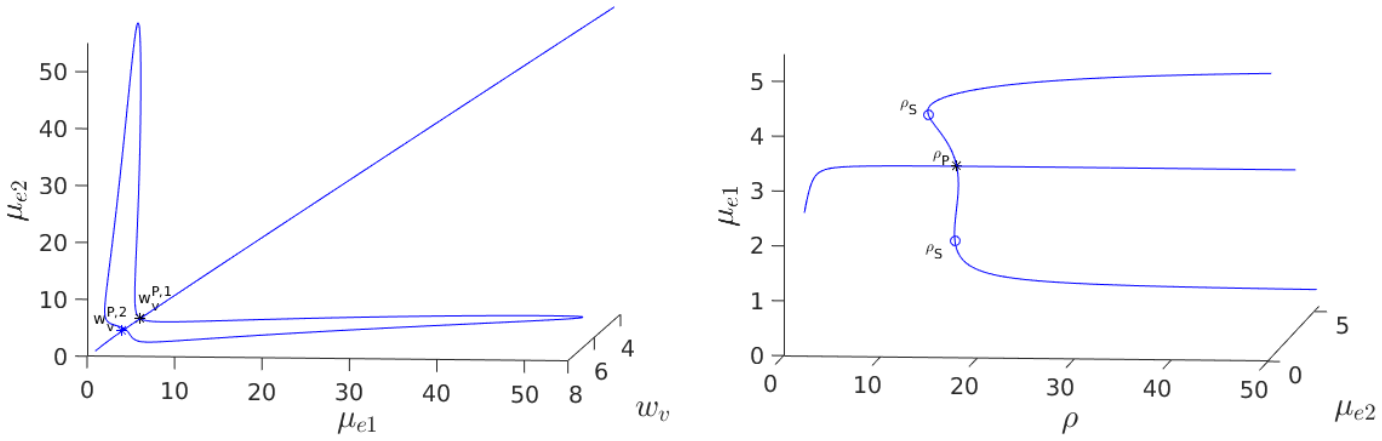

Figure 12: 3-D Bifurcation diagram, computed from (4.8) using MatCont [7], for symmetric and asymmetric steady-states of a two-cell ring pattern with ring radius $r = 0.5$ and with RM kinetics (4.7). Left: 3-D Plot of (μ_{e1}, μ_{e2}) versus the kinetic parameter w_v in (4.7) at a fixed $\rho = d_v/d_u = 15$, showing that asymmetric steady-states occur inside the degenerate pitchfork bubble delimited by $w_v^{P,1} \approx 6.88285$ and $w_v^{P,2} \approx 7.08723$. Note that the bubble lobes are stretching into decreasing w_v and that there exists hysteresis at $w_v^{P,2}$. Right: In terms of ρ, a supercritical pitchfork bifurcation from the symmetric branch occurs when $w_v = w_v^{P,2} \approx 7.08723$. The asymmetric branches are linearly stable past this bifurcation threshold in ρ. Parameters: $D_u = D_v = 1, \sigma_u = \sigma_v = 0.1, \varepsilon = 0.03, c_u = c_v = 1, q_u = 1/100, q_v = 7, a_1^u = 600, a_2^u = 6, b_1^u = 100, b_2^u = 1/10$, and $d_u = 0.14$.

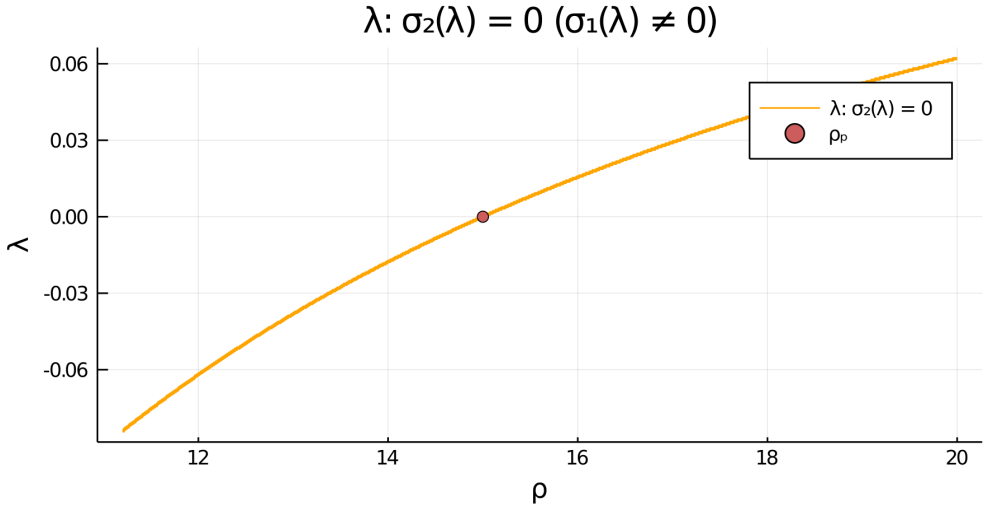

Figure 13: For the two-cell system with RM kinetics (4.7) and parameters as in the caption of Figure 12 with $w_v = w_v^{P,2}$, we plot the eigenvalue λ, satisfying $\sigma_2(\lambda) = 0$ in (3.20), versus ρ that determines the linear stability of the symmetric steady-state solution branch to eigenperturbations of the form $\mathbf{q}_2 = (1, -1)^T$. We observe that the symmetric steady-state branch is unstable only for $\rho > \rho_p = 15$. There is no root to $\sigma_1(\lambda) = 0$ on this range.

4.3 FitzHugh-Nagumo reaction kinetics

Finally, we consider a ring pattern for the bulk-cell system (2.3) with two cells and with FitzHugh-Nagumo (FN) intracellular reaction kinetics [17]. The uncoupled intracellular kinetics are

$$\dot{\mu}(t) = \mu - q(\mu-2)^3 + 4 - \eta \equiv f(\mu,\eta)\,, \qquad \dot{\eta}(t) = \delta z\mu - \delta\eta \equiv g(\mu,\eta)\,, \tag{4.11}$$

with $q>0$, $\delta>0$ and $z>0$. Since g has the form in (2.14), we identify that $g_1(\mu)=\delta z$ and $g_2=\delta$.

We will choose a parameter set for which there is a unique linearly stable steady-state of the intra-compartmental dynamics (4.11). From (2.16), all steady-states of the bulk-cell model for a two-cell ring pattern are obtained from the nonlinear algebraic problem

$$\begin{array}{rcl} f(\mu_{e1},\delta z\mathbf{e}_1^T(\delta I+\Theta_v)^{-1}(\mu_{e1},\mu_{e2})^T) - \mathbf{e}_1^T\Theta_u(\mu_{e1},\mu_{e2})^T &=& 0 \\ f(\mu_{e2},\delta z\mathbf{e}_2^T(\delta I+\Theta_v)^{-1}(\mu_{e1},\mu_{e2})^T) - \mathbf{e}_2^T\Theta_u(\mu_{e1},\mu_{e2})^T &=& 0\,. \end{array} \tag{4.12}$$

The symmetric steady-state solution branch, as characterized by (2.20), is obtained from the root μ_e of the cubic equation

$$\mu_e - q(\mu_e-2)^3 + 4 - \frac{\delta z\mu_e}{\delta+\alpha_v} - \alpha_u\mu_e = 0\,, \tag{4.13}$$

where α_u and α_v are given in (2.19). The symmetry-breaking bifurcation condition (2.30) along the symmetric steady-state solution branch yields that

$$1 - 3q(\mu_e-2)^2 - \frac{\delta z}{\delta+\alpha_{v,2}^{\perp}} - \alpha_{u,2}^{\perp} = 0 \qquad \Leftrightarrow \qquad z(\mu_e) = \frac{\delta+\alpha_{v,2}^{\perp}}{\delta}\left(1 - 3q(\mu_e-2)^2 - \alpha_{u,2}^{\perp}\right)\,,$$

where $\alpha_{u,2}^{\perp}$ and $\alpha_{v,2}^{\perp}$ are defined in (2.31). We substitute $z(\mu_e)$ into (4.13), and solve the resulting equation numerically for μ_e. For $\rho=150$, and with the parameters as in the caption of Figure 14, we obtain that there are two supercritical pitchfork bifurcation points $z_{P,1}$ and $z_{P,2}$ on the symmetric steady-state branch. The linearly stable asymmetric steady-state branches that exist on the range $z_{P,1}<z<z_{P,2}$ between the two pitchfork points are shown in the left panel of Figure 14. When $z=z_{P,2}$, we observe from the bifurcation diagram in the right panel of Figure 14, together with the eigenvalue computations in Figure 15, that the symmetry-breaking bifurcation is supercritical in terms of ρ.

Next, we illustrate that the bulk-cell model with FN kinetics can also exhibit oscillatory instabilities for in-phase perturbations of the symmetric steady-state. In Figure 16 we plot the bifurcation diagram of μ_{e1} versus z for the same parameter set as in the caption of Figure 14 except that the bulk degradation rates have been decreased slightly to $\sigma_u=\sigma_v=0.9$. We observe that there are now two Hopf bifurcation values $z_{H,1}$ and $z_{H,2}$ of z along the symmetric steady-state branch for the in-phase mode that lie within the interval delimited by the two pitchfork bifurcation points. In the right panel of Figure 16, we plot the real and imaginary parts of the complex-valued root of $\sigma_1(\lambda)=0$, as computed from (3.20), which shows that $\mathrm{Re}(\lambda)>0$ and $\mathrm{Im}(\lambda)\neq 0$ when $z_{H,1}<z<z_{H,2}$. This leads to the possibility of a synchronous oscillatory instability. As a result, on the range $z_{H,1}<z<z_{H,2}$, the symmetric steady-state solution branch is unstable to both anti-phase and in-phase perturbations. However, as seen from the right-panel of Figure 16, where we also plot the growth rate λ for the anti-phase mode as obtained by setting $\sigma_2(\lambda)=0$ in (3.20), the anti-phase instability has a larger growth rate than the in-phase instability.

4.4 Numerical experiments with closely-spaced cells: GM kinetics

We now briefly explore, from full PDE simulations of (2.3), symmetry-breaking behavior leading to stable asymmetric patterns that can occur for closely spaced cells when the ratio $\rho=d_v/d_u$ is increased. For realistic modeling of pattern formation properties of biological tissues one needs to consider the situation where cells are closely spaced in the sense that the cell radii are either comparable to the distance between the cells, or that there are only narrow gaps between cells. Although the asymptotic theory of §2 and §3 is no longer valid for such closely spaced cell arrangements, the FlexPDE simulations of (2.3) shown below reveal a similar qualitative solution behavior as we have analyzed for spatially segregated cells. More specifically, although we no longer have

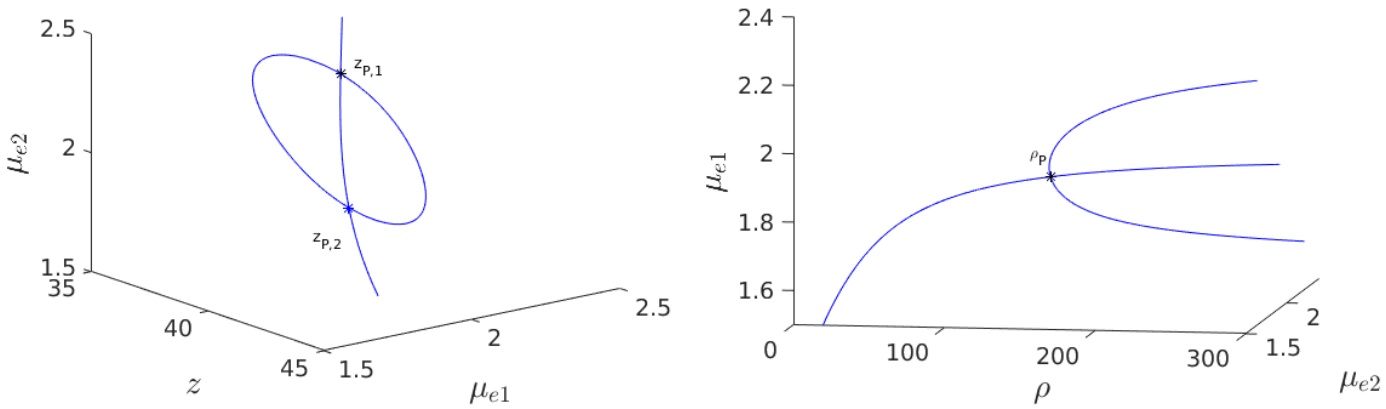

Figure 14: 3-D Bifurcation diagram, computed from (4.12) using MatCont [7], for symmetric and asymmetric steady-states of a two-cell ring pattern with ring radius $r = 0.5$ and with FN kinetics (4.11). Left: 3-D Plot of (μ_{e1}, μ_{e2}) showing that asymmetric steady-states occur inside the supercritical pitchfork bubble delimited by $z_{P,1} \approx 36.75458$ and $z_{P,2} \approx 41.26889$ when $\rho = d_v/d_u = 150$. Right: Supercritical pitchfork bifurcation from the symmetric branch occurs at $\rho_p = 150$ when $z = z_{P,2}$. Linearly stable asymmetric branches exist past this threshold in ρ. Parameters: $D_u = 1, D_v = 4, \sigma_u = \sigma_v = 1, \varepsilon = 0.03, r = 0.5, q = 1, \delta = 0.1$, and $d_u = 0.04$.

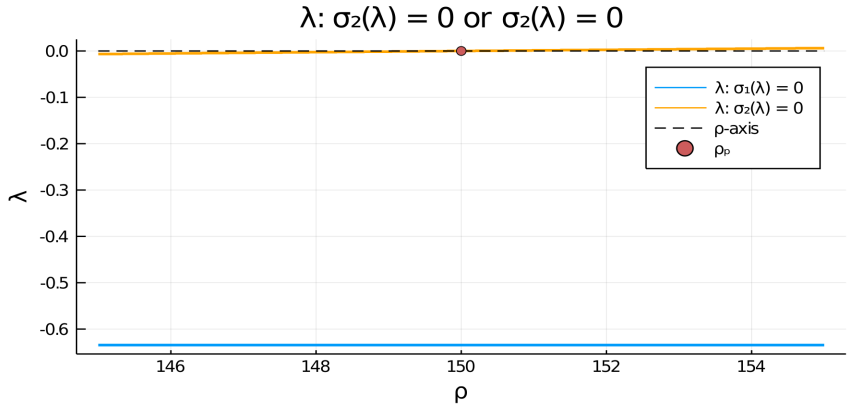

Figure 15: For the two-cell system with FN kinetics (4.11) and parameters as in the caption of Figure 14 with $z = z_{P,2}$, we plot the numerically computed eigenvalue λ, satisfying $\sigma_2(\lambda) = 0$ in (3.20), versus ρ. Since $\lambda > 0$ only on the range $\rho > \rho_p = 150$, we conclude that the symmetric steady-state solution is linearly stable to anti-phase eigenperturbations of the form $\mathbf{q}_2 = (1, -1)^T$ only when $\rho < \rho_p = 150$. Moreover, since the root to $\sigma_1(\lambda) = 0$ satisfies $\lambda < 0$, we conclude that the symmetric steady-state branch is always linearly stable to in-phase eigenperturbations of the symmetric steady-state.

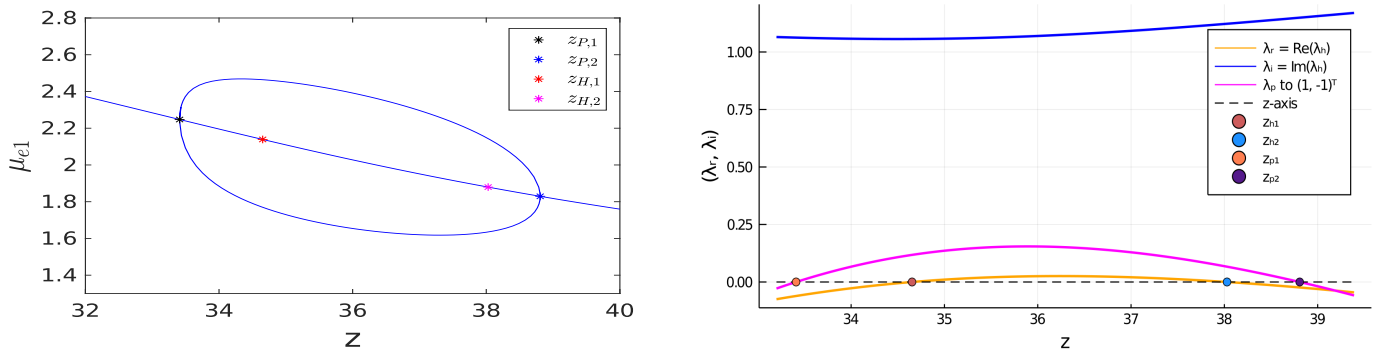

Figure 16: Left panel: Bifurcation diagram of μ_{e1} versus z, computed from (4.12) using MatCont [7], for symmetric and asymmetric steady-states of a two-cell ring pattern with the same parameters as in the left panel of Figure 14 except that now the degradation rates are decreased slightly to $\sigma_u = \sigma_v = 0.9$. For this parameter set, there are Hopf bifurcation points associated with in-phase perturbations of the symmetric steady-state that emerge at $z = z_{H,1} \approx 34.65328$ and $z = z_{H,2} \approx 38.02834$ between the two symmetry-breaking pitchfork bifurcation points located at $z = z_{P,1} \approx 33.41022$ and $z = z_{P,2} \approx 38.80742$. Right panel: the root λ of $\sigma_2(\lambda) = 0$ versus z (pink curve), as computed from (3.20), shows that the symmetric steady-state solution branch is unstable to anti-phase perturbations on the range $z_{P,1} < z < z_{P,2}$. The plotted real and imaginary parts of the complex-valued root $\lambda_h \equiv \lambda_r + i\lambda_i$ to $\sigma_1(\lambda_h) = 0$, from (3.20), shows that $\mathrm{Re}(\lambda_h) > 0$ on the range $z_{H,1} < z < z_{H,2}$. On this range of z, a synchronous oscillatory instability of the symmetric steady-state solution can also occur, but it has a smaller growth rate than that for the anti-phase mode.

an analytical theory to predict a bifurcation diagram of all steady-state solutions, our full PDE numerical results suggest that stable symmetric steady-states occur only when ρ is below some threshold. When ρ exceeds some symmetry-breaking threshold, stable asymmetric steady-states will be the preferred state. Our numerical results suggest that the critical threshold of ρ that is needed to establish this symmetry-breaking behavior for closely spaced cells is smaller than that needed for spatially segregated cells, if in fact such a threshold exists.

To illustrate this, in Figure 17 we take two closely spaced cells centered near the origin that have a minimum separation of 0.002. The degradation rates, cell radius, and the value of d_u used for Figure 17 are the same as in Table 3, where bifurcation values were given for the two-cell arrangement at different ratios of D_v/D_u with $D_u = 5$ and for a ring radius $r = 0.5$. In the cell arrangement in Figure 17, the only difference is that the two cells are now much more closely spaced than in Table 3 and we fix $D_v/D_u = 0.3$ and $D_u = 5$. For these parameter values, we observe from Table 3 that no symmetry-breaking bifurcations are possible for this diffusivity ratio when the ring radius is $r = 0.5$. However, as suggested from the results shown in Figure 17, when the cells are closely spaced there is a symmetry-breaking pitchfork bifurcation point that occurs on the range $3 < \rho < 8$. We remark that, rather surprisingly, if we use the symmetry-breaking bifurcation condition (4.6) from the asymptotic theory for this case of two-closely spaced cells it predicts that $\rho_p \approx 6.16$, which lies within the range $3 < \rho < 8$. However, we emphasize that the asymptotic theory is not valid for closely-spaced cells.

Finally, in Figure 18 we show that the stable asymmetric steady-state patterns can also occur for three closely-spaced cells when ρ exceeds some threshold.

5 Discussion

We have analyzed symmetry-breaking behavior associated with the PDE-ODE bulk-cell model (2.3) where identical two-component intra-compartmental reactions occur only within a disjoint collection of small circular compartments, or "cells", of a common radius within a bounded 2-D domain. In the bulk, or extra-cellular, medium two bulk species with comparable diffusivities and bulk degradation rates diffuse and globally couple the spatially segregated intracellular reactions. The bulk species are coupled to the intracellular species through an exchange across the compartment boundaries, as modeled by a Robin boundary condition that depends on certain mem-

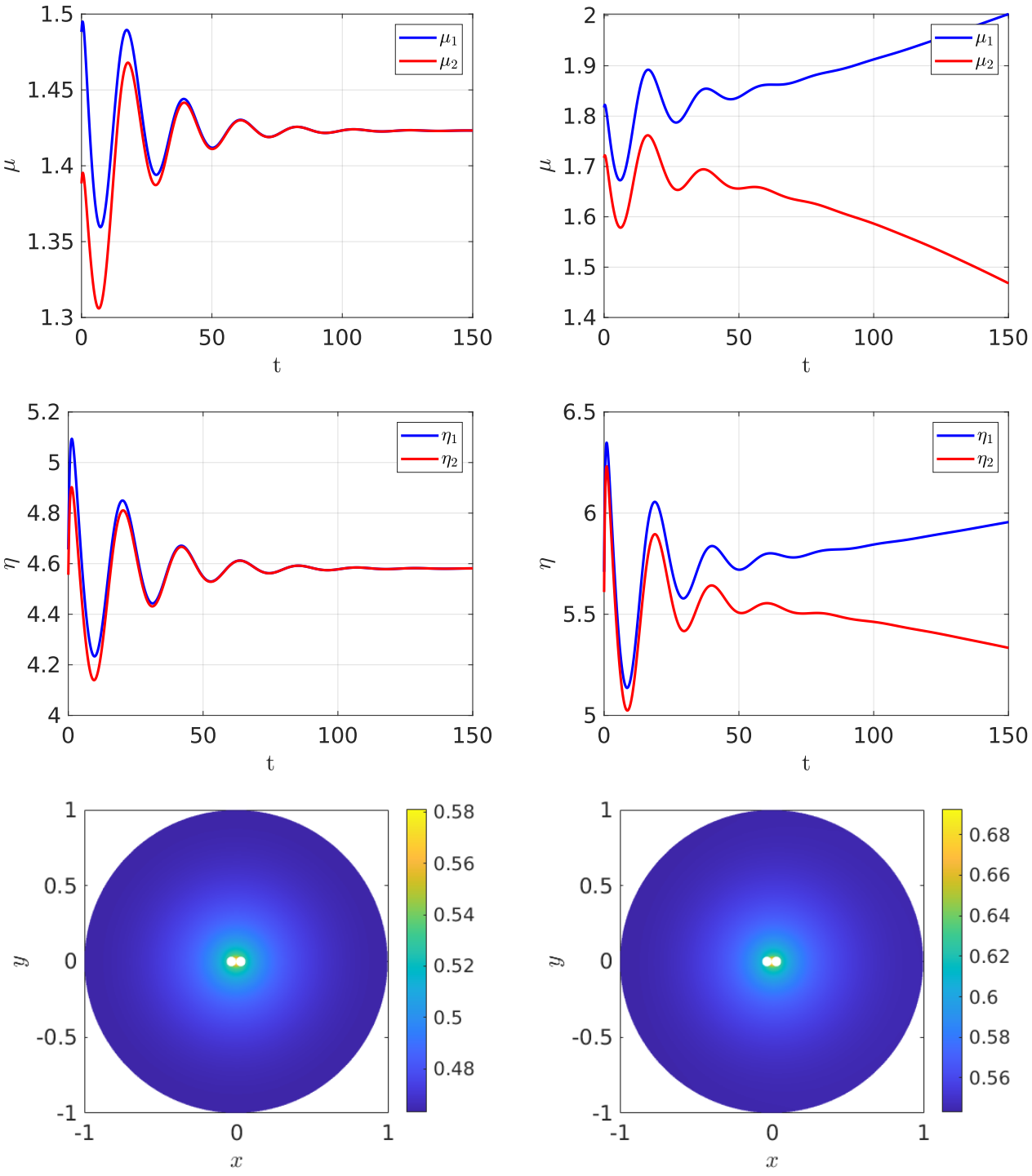

Figure 17: Full numerical simulation results of (2.3) with FlexPDE [13] for GM kinetics (4.3) with two closely spaced cells centered on a ring of radius $r = 0.031$ and with minimum cell separation of 0.002. The other parameters are the same as in Table 3. The only difference here is that the cells are now much more closely spaced. Left: convergence to a stable symmetric steady-state solution when $\rho = 3$. Right: convergence to a stable asymmetric steady-state soluton for $\rho = 8$ when starting with a symmetric initial condition. Parameters: $D_u = 5$, $D_v = 1.5$, $\sigma_u = \sigma_v = 0.6$, $d_u = 0.08$, and $\varepsilon = 0.03$.

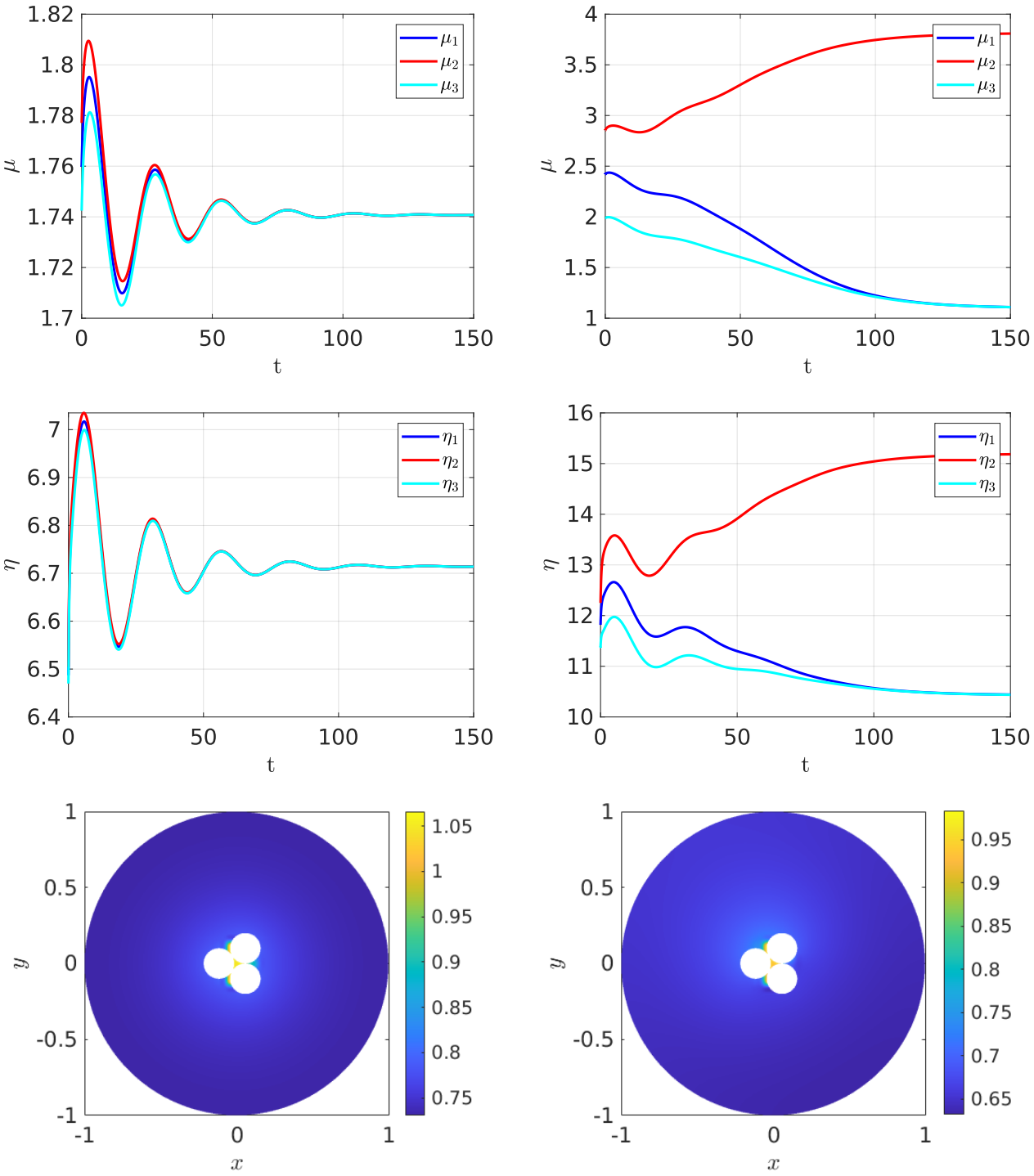

Figure 18: Full numerical simulation results of (2.3) with FlexPDE [13] for GM kinetics (4.3) with three closely spaced cells with cell centers located on the vertices of an equilateral triangle centered at the origin. The ring radius is $r = 0.2\sqrt{3}/6$. Left: convergence to a symmetric steady-state when $\rho = 5$. Right: convergence to an asymmetric steady-state when $\rho = 10$. Parameters: $D_u = D_v = 5, \sigma_u = \sigma_v = 0.6, d_u = 0.05, \varepsilon = 0.099$. The cells have a minimum separation of 0.002.

brane reaction rates. In the limit of a small cell radius, we have used a singular perturbation methodology to derive a nonlinear algebraic system (2.13) characterizing all the steady-states for the bulk-cell model (2.3). Moreover, the linear stability properties of the steady-state solutions of the bulk-cell model were shown to be determined by the nonlinear matrix eigenvalue problem (3.12) of size $2m \times 2m$, where m is the number of compartments. A root-finding condition on the determinant of this matrix yields the discrete eigenvalues of the linearization (3.1) around an arbitrary steady-state solution, as defined by the set (3.13).

We have shown that the steady-state and linear stability theory simplifies considerably for a **symmetric cell arrangement**, as characterized by Definition 2.1, and when one of the intracellular species has a linear dependence of the form (2.14). In this more restricted scenario, we have shown that a symmetric steady-state solution, in which the steady-states of the intracellular species are the same for each cell, will exist if the scalar nonlinear algebraic equation (2.20) has a solution. We emphasize that since our bulk-cell model does not admit spatially homogeneous steady-state solutions that can be analyzed by a simple Turing-type linear stability approach [58], this symmetric steady-state solution of the bulk-cell model (2.3) represents the **base state** in our construction. Instabilities and bifurcations associated with this base state are challenging to analyze owing to the fact that the base state is not spatially uniform. Asymmetric steady-state solutions, as determined from (2.16), were shown to bifurcate from the symmetric steady-state solution branch whenever the algebraic criterion (2.29) is satisfied at some point on the symmetric branch. For a symmetric cell arrangement, the linear stability properties of the symmetric and asymmetric steady-state solution branches are characterized by (3.21) and the roots of the nonlinear matrix eigenvalue problem (3.18), respectively.

We have implemented our steady-state and linear stability theory for a specific symmetric cell arrangement in which two cells are equally spaced on a ring concentric within a unit disk, and where we have specified either Gierer-Meinhardt, Rauch-Millonas, or FitzHugh-Nagumo intracellular reactions, which all have the simplified form in (2.14). By using parameter continuation numerical software [7] to implement the asymptotic theory, we have shown that the symmetric steady-state solution branch can undergo **symmetry-breaking pitchfork bifurcations**, leading to linearly stable asymmetric patterns, even when the two bulk diffusing species have identical diffusivities and degradation rates. Overall, we have shown that it is the magnitude of the ratio of the reaction rates for the two bulk species to the cell membranes that determines whether stable asymmetric patterns can occur. This membrane reaction rate ratio threshold condition for the emergence of symmetry-breaking bifurcations is in marked contrast to the well-known large diffusivity ratio threshold condition for pattern formation from a spatially uniform state that is typically derived by a Turing stability analysis for two-component activator-inhibitor RD systems. For FitzHugh-Nagumo and Rauch-Millonas kinetics we have also shown that stable asymmetric patterns can also emerge from a symmetric steady-state pattern at a fixed, but large, membrane reaction rate ratio when a control parameter in the intracellular kinetics is varied. Our theoretical predictions of symmetry-breaking behavior leading to linearly stable asymmetric patterns for a symmetric two-cell arrangement were confirmed through full time-dependent PDE computations of (2.3).

We now briefly relate our theoretical results to some qualitative behavior that has been suggested in chemical and biological applications. Firstly, compartmental-reaction diffusion models of the form (2.3) could potentially be useful for theoretically modeling the collective behavior that occurs for a microemulsion consisting of Belousov-Zhabotinsky (BZ) chemical reactants that are confined within small aqueous droplets that is dispersed in oil [57] (see also [12], [5]). In this experimental set-up, polar BZ reactants and a catalyst are confined within small immobile droplets, while two non-polar intermediate species generated during the reaction can be transported across the droplet boundaries. These intermediate species diffuse across the domain, with comparable diffusivities, and provide the mechanism for inter-drop coupling [57]. The recent experimental study of [5] has suggested that it is the relative magnitude of the membrane reaction rates of these intermediates on the droplet boundaries that plays a key role for determining pattern-forming properties for BZ microemulsions. Secondly, with regards to the transport of biological morphogens, it has been suggested in [39] that a differential reaction rate ratio on the cell boundaries for two morphogen species with comparable diffusivities can yield the large **effective** diffusivity ratio that is needed for pattern formation and symmetry-breaking in tissues. This membrane attachment mechanism, which reduces the effective diffusivity of one of the morphogens and is referred to in [39] as a **binding-mediated hindrance** diffusion process, may be relevant in many biological applications. Moreover, detailed intracellular mechanisms in biological cells, such as signaling pathways and gene expression rate constants, may also play a

pivotal role in large-scale pattern-forming properties of biological tissues [39]. By way of qualitiative comparison, our theoretical analysis of the 2-D bulk-cell model (2.3) for a very simple 2-cell pattern has revealed that a large membrane reaction rate ratio, together possibly with changes in a parameter in the intracellular kinetics, can trigger the emergence of stable asymmetric steady-state patterns that bifurcate from a symmetry steady-state. However, owing to the complexity of the analysis needed for (2.3), where certain Green's matrices were found to be central to the analysis, it appears rather intractable analytically to isolate via a simple scaling analysis an **effective diffusivity** for the bulk species that incorporates the membrane reaction rates.

Although we have only applied our theoretical framework to a simple two-cell arrangement, it is rather straightforward to numerically implement the steady-state and linear stability theory for a symmetric cell arrangement with a much larger number of cells. For this scenario, the symmetric steady-state solutions are again determined by the scalar nonlinear algebraic equation (2.20) and the linear stability properties of this steady-state are readily studied by computing the union of all the roots of the scalar problems $\sigma_j(\lambda) = 0$, for $j \in \{1, \ldots, m\}$, in (3.20) that comprise the set (3.21) that approximates the discrete eigenvalues of the linearization (3.1) of (2.3) around the steady-state. However, for an arbitrary spatial arrangement of a large number of cells, one key impediment for implementing the linear stability theory for steady-state solutions is with regards to numerically computing the eigenvalues λ from a root-finding condition on the determinant of the full $2m \times 2m$ GCEP matrix $\mathcal{M}(\lambda)$ in (3.12). This matrix is non-Hermitian, is not sparse, and has an intricate dependence on λ through the Green's matrices. In contrast to the availability of efficient numerical solution strategies for nonlinear matrix eigenvalue problems with special structure, as was discussed in [22], [3] and [2], it appears to a significant open challenge to develop efficient numerical methods to determine all such eigenvalues λ for which $\mathcal{M}(\lambda)$ is a singular matrix when m is large. Recall that if there are any such eigenvalues in $\mathrm{Re}(\lambda) > 0$, the steady-state for (2.3) is unstable.

A few other open problems related to our analysis are as follows. Firstly, it would be interesting to analyze symmetry-breaking bifurcation for (2.3) on $\mathbb{R}^2$ where identical cells of small radii are centered at the lattice points of an arbitrary Bravais lattice. In this periodic setting, it should be possible to analyze symmetry-breaking bifurcations of a periodic steady-state solution by using Floquet-Bloch theory, combined with the explicit analytical formulae for the reduced-wave Bloch Green's function as derived in [26]. Secondly, it would be interesting to develop an extension of our asymptotic approach to treat closely-spaced cell configurations that are more relevant to modeling pattern-forming properties in biological tissues. Our numerical results shown in §4.4 have suggested that only a smaller membrane reaction rate ratio is needed to initiate symmetry-breaking behavior for closely-spaced cells than for arrangements with more spatially segregated cells. To theoretically analyze pattern-forming properties of the bulk-cell model with closely-spaced cells, an extension of the approach developed in [27] to analyze the mean first passage time for a cluster of small traps may be fruitful. Finally, it would be interesting to formulate and analyze a related bulk-cell model where the chemical reactions occur on the boundaries of a collection of small compartments, rather than in the interior of the compartments. In this scenario, chemical species produced on the membrane can then detach and diffuse in the bulk medium. Such an extension is relevant for analyzing collective behavior that occurs for dynamically reactive solid pellets that are chemically coated and are coupled through a bulk diffusion field (cf. [53], [54], [56], [55]).

A Non-dimensionalization

Here we non-dimensionalize (2.2) to obtain the PDE-ODE system (2.3). Let $[z]$ denote the unit of some variable z. In the SI unit system, we have

$$\begin{array}{rclrclrclrcl} [U] &=& \frac{\text{moles}}{\text{m}^2}\,, & [D_U] &=& \frac{\text{m}^2}{\text{s}}\,, & [\kappa_U] &=& \frac{1}{\text{s}}\,, & [T] &=& \text{s}\,, & [X] &=& \text{m}\,, \\ [M_j] &=& \text{moles}\,, & [\kappa_R] &=& \frac{1}{\text{s}}\,, & [\mu_c] &=& \text{moles}\,, & [\beta_{U,1}] &=& \frac{\text{m}}{\text{s}}\,, & [\beta_{U,2}] &=& \frac{1}{\text{m}\,\text{s}}\,. \end{array}$$

Letting L denote the length-scale of the domain, we introduce the dimensionless variables $u \equiv L^2 U/\mu_c$, $v \equiv L^2 V/\mu_c$, $t \equiv \kappa_R T$, $\mathbf{x} \equiv X/L$, $\mu_j \equiv M_j/\mu_c$, and $\eta_j \equiv H_j/\mu_c$. Then, we obtain that

$$\begin{array}{rcl} \kappa_R\,\partial_t U &=& \frac{D_U}{L^2}\,\Delta_{\mathbf{x}} U - \kappa_U U\,, \\ \kappa_R\,\partial_t V &=& \frac{D_V}{L^2}\,\Delta_{\mathbf{x}} V - \kappa_V V\,, \end{array} \qquad \Leftrightarrow \qquad \begin{array}{rcll} \partial_t u &=& D_u \Delta_{\mathbf{x}} u - \sigma_u u, & \mathbf{x} \in \Omega \backslash \bigcup_{j=1}^m \Omega_j\,, \\ \partial_t v &=& D_v \Delta_{\mathbf{x}} v - \sigma_v v, & \mathbf{x} \in \Omega \backslash \bigcup_{j=1}^m \Omega_j\,, \end{array}$$

where we have defined the dimensionless effective diffusivities D_u and D_v and degradation rates σ_u and σ_v by

$$D_u \equiv \frac{D_U}{L^2\kappa_R}\,, \qquad \sigma_u \equiv \frac{\kappa_U}{\kappa_R}\,, \qquad D_v \equiv \frac{D_V}{L^2\kappa_R}\,, \qquad \sigma_v \equiv \frac{\kappa_V}{\kappa_R}\,.$$

Since we assume that the common radius, denoted by L_c, of the cells is much smaller than the domain length-scale L, we introduce $\varepsilon \ll 1$ by $\varepsilon = L_c/L \ll 1$.

Next, by non-dimensionalizing the Robin boundary conditions in (2.2), we obtain

$$\begin{array}{rcl} \frac{D_U}{L}\frac{\mu_c}{L^2}\,\partial_{n_{\mathbf{x}}}u &=& \beta_{U,1}\,\frac{\mu_c}{L^2}u - \beta_{U,2}\,\mu_c\mu_j\,, \\ \frac{D_V}{L}\frac{\mu_c}{L^2}\,\partial_{n_{\mathbf{x}}}v &=& \beta_{V,1}\,\frac{\mu_c}{L^2}v - \beta_{V,2}\,\mu_c\eta j\,, \end{array} \qquad \Leftrightarrow \qquad \begin{array}{rcll} \varepsilon D_u\partial_{n_{\mathbf{x}}}u &=& d_1^u u - d_2^u\mu_j, & \mathbf{x}\in\partial\Omega_j\,, \\ \varepsilon D_v\partial_{n_{\mathbf{x}}}v &=& d_1^v v - d_2^v\eta_j, & \mathbf{x}\in\partial\Omega_j\,, \end{array}$$

where we have defined d_1^u, d_2^u, d_1^v, and d_2^v by

$$d_1^u \equiv \frac{\beta_{U,1}}{\kappa_R L}\varepsilon\,, \qquad d_2^u \equiv \frac{\beta_{U,2}L}{\kappa_R}\varepsilon\,, \qquad d_2^v \equiv \frac{\beta_{V,1}}{\kappa_R L}\varepsilon\,, \qquad d_2^v \equiv \frac{\beta_{V,2}L}{\kappa_R}\varepsilon\,.$$

Here, in order that there is an $\mathcal{O}(1)$ exchange across the cell membranes we have assumed that $\frac{\beta_{U,1}}{\kappa_R L}$, $\frac{\beta_{U,2}L}{\kappa_R}$, $\frac{\beta_{V,1}}{\kappa_R L}$ and $\frac{\beta_{V,2}L}{\kappa_R}$ are all $\mathcal{O}\left(\varepsilon^{-1}\right)$.

Lastly, we non-dimensionalize the intracellular reaction kinetics in (2.2) by

$$\begin{array}{rcl} \kappa_R\mu_c\,\frac{d}{dt}\mu_j &=& \kappa_R\mu_c\,f(\mu_j,\eta_j) + \int_{\partial\Omega_j}\left(\beta_{U,1}\frac{\mu_c L}{L^2}\,u - \beta_{U,2}\mu_c L\,\mu_j\right)\,dS_{\mathbf{x}}\,, \\ \kappa_R\mu_c\,\frac{d}{dt}\eta_j &=& \kappa_R\mu_c\,g(\mu_j,\eta_j) + \int_{\partial\Omega_j}\left(\beta_{V,1}\frac{\mu_c L}{L^2}\,v - \beta_{V,2}\mu_c L\,\eta_j\right)\,dS_{\mathbf{x}}\,, \end{array}$$

which yields the dimensionless intracellular reactions

$$\frac{d\mu_j}{dt} = f(\mu_j,\eta_j) + \frac{1}{\varepsilon}\int_{\partial\Omega_j}\left(d_1^u\,u - d_2^u\,\mu_j\right)\,dS_{\mathbf{x}}\,, \qquad \frac{d\eta_j}{dt} = g(\mu_j,\eta_j) + \frac{1}{\varepsilon}\int_{\partial\Omega_j}\left(d_1^v\,v - d_2^v\,\eta_j\right)\,dS_{\mathbf{x}}\,,$$

for each $j\in\{1,...,m\}$. This completes the derivation of (2.3).

B Reduced-wave Green's function for the unit disk

When Ω is the unit disk, the reduced-wave Green's function $G_\omega(\mathbf{x};\xi)$ and its regular part, satisfying (2.9) can be determined analytically using separation of variables as (see equations (6.10) and (6.11) of [20])

$$G_\omega(\mathbf{x};\xi) = \frac{1}{2\pi}K_0\left(\omega|\mathbf{x}-\xi|\right) - \frac{1}{2\pi}\sum_{n=0}^{\infty}\beta_n\cos\left(n(\psi-\psi_0)\right)\frac{K_n'(\omega)}{I_n'(\omega)}I_n\left(\omega|\mathbf{x}|\right)I_n\left(\omega|\xi|\right)\,, \tag{B.1a}$$

$$R_\omega(\xi) = \frac{1}{2\pi}\left(\log 2 - \gamma_e - \log\omega\right) - \frac{1}{2\pi}\sum_{n=0}^{\infty}\beta_n\frac{K_n'(\omega)}{I_n'(\omega)}\left[I_n\left(\omega|\xi|\right)\right]^2\,, \tag{B.1b}$$

where $\gamma_e \approx 0.5772$ is Euler's constant, and $I_n(z)$ and $K_n(z)$ are the modified Bessel functions of the first and second kind of order n, respectively. In (B.1), $\beta_0 \equiv 1$, $\beta_n \equiv 2$ for $n \geq 1$, while $\mathbf{x} \equiv |\mathbf{x}|(\cos\psi,\sin\psi)^T$, and $\xi \equiv |\xi|(\cos\psi_0,\sin\psi_0)^T$.

For a ring pattern where the cell centers $\mathbf{x}_k$ for $k\in\{1,\ldots,m\}$, are equidistantly spaced on a ring of radius r concentric within the unit disk, as in (4.1), all the Green's matrices used in the steady-state and linear stability analysis are circulant and symmetric matrices. As a result, each such matrix spectrum is available analytically.

Following Appendix A of [50], for an $m\times m$ circulant matrix $\mathcal{A}$, with possibly complex-valued matrix entries, its complex-valued eigenvectors $\tilde{\mathbf{v}}_j$ and eigenvalues α_j are $\alpha_j = \sum_{k=1}^{m}\mathcal{A}_{1k}\omega_j^{k-1}$ and $\tilde{\mathbf{v}}_j = \left(1, Z_j, \ldots, Z_j^{m-1}\right)^T$, for $j\in\{1,\ldots,m\}$. Here $Z_j \equiv \exp\left(\frac{2\pi i(j-1)}{m}\right)$ and $\mathcal{A}_{1k}$, for $k\in\{1,\ldots,m\}$, are the elements of the first row of $\mathcal{A}$. Since $\mathcal{A}$ is also a symmetric matrix, we have $\mathcal{A}_{1,j} = \mathcal{A}_{1,m+2-j}$, for $j\in\{2,\ldots,\lceil m/2\rceil\}$, where the ceiling function

$\lceil x \rceil$ is defined as the smallest integer not less than x. Therefore, $\alpha_j = \alpha_{m+2-j}$, for $j \in \{2, \ldots, \lceil m/2 \rceil\}$, so that there are $m-1$ eigenvalues with a multiplicity of two when m is odd, and $m-2$ such eigenvalues when m is even. As a result, we conclude that $\frac{1}{2}\left[\tilde{\mathbf{v}}_j + \tilde{\mathbf{v}}_{m+2-j}\right]$ and $\frac{1}{2i}\left[\tilde{\mathbf{v}}_j - \tilde{\mathbf{v}}_{m+2-j}\right]$ are two independent real-valued eigenvectors of $\mathcal{A}$, corresponding to the eigenvalues of multiplicity two. In summary, the matrix spectrum of a circulant and symmetric matrix $\mathcal{A}$, where the eigenvectors have been normalized by $\mathbf{v}_j^T \mathbf{v}_j = 1$, is

$$\alpha_j = \sum_{k=1}^{m} \mathcal{A}_{1k} \cos\left(\theta_j (k-1)\right) , \quad j \in \{1, \ldots, m\} ; \qquad \theta_j \equiv \frac{2\pi(j-1)}{m} ; \qquad \mathbf{v}_1 = \frac{1}{\sqrt{m}} \mathbf{e} , \tag{B.2a}$$

$$\mathbf{v}_j = \sqrt{\frac{2}{m}} \left(1, \cos\left(\theta_j\right), \ldots, \cos\left(\theta_j (m-1)\right)\right)^T , \quad \mathbf{v}_{m+2-j} = \sqrt{\frac{2}{m}} \left(0, \sin\left(\theta_j\right), \ldots, \sin\left(\theta_j (m-1)\right)\right)^T \tag{B.2b}$$

for $j \in \{2, \ldots, \lceil m/2 \rceil\}$, where $\theta_j \equiv 2\pi(j-1)/m$. When m is even, there is an additional normalized eigenvector of multiplicity one given by $\mathbf{v}_{m/2+1} = m^{-1/2}(1, -1, 1, \ldots, -1)^T$.

References

[1] R. E. Baker, E. A. Gaffney, and P. K. Maini. Partial differential equations for self-organization in cellular and developmental biology. *Nonlinearity*, 21(11):R251, 2008.

[2] T. Betcke, N. G. Highan, V. Mehrmann, G. M. N. Porzio, C. Schröder, and Tisseur F. NLEVP: A collection of nonlinear eigenvalue problems. Users' guide. *MIMS EPring 2011.117, Manchester Institue for Mathematical Sciences, The University of Manchester, UK*, updated 2019.

[3] T. Betcke, N. G. Highan, V. Mehrmann, C. Schröder, and Tisseur F. NLEVP: A collection of nonlinear eigenvalue problems. *ACM Trans. Math. Software*, 39(2):7.1–7.28, 2013.

[4] J. Bezanson, S. Karpinski, V. B. Shah, and A. Edelman. Julia: A fast dynamic language for technical computing. *arXiv preprint arXiv:1209.5145*, 2012.

[5] M. A. Budroni, K. Torbensen, S. Ristori, Abou-Hassan A., and F. Rossi. Membrane structure drives synchronization patterns in arrays of diffusively coupled self-oscillating droplets. *J. Phys. Chem. Lett*, 11(6):2014–2020, 2020.

[6] D. Cusseddu, L. Edelstein-Keshet, J. A. Mackenzie, S. Portet, and A. Madzvamuse. A coupled bulk-surface model for cell polarisation. *J. Theor. Biol.*, 481:119–135, 2019.

[7] A. Dhooge, W. Govaerts, and Y. A Kuznetsov. MatCont: a MATLAB package for numerical bifurcation analysis of ODEs. *ACM Trans. Math. Software (TOMS)*, 29(2):141–164, 2003.

[8] L. Diambra, V. R. Senthivel, D. B. Menendez, and M. Isalan. Cooperativity to increase Turing pattern space for synthetic biology. *AVS Synthetic Biology*, 4:177–186, 2015.

[9] X. Diego, L. Marcon, P. Müller, and J. Sharpe. Key features of Turing systems are determined purely by network topology. *Phys. Rev. X*, 8:021071, 2018.

[10] E. Dulos, J. Boissonade, J. J. Perraud, B. Rudovics, and P. De Kepper. Chemical morphogenesis: Turing patterns in an experimental chemical system. *Acta Biotheor.*, 44:249, 1996.

[11] C. M. Elliott, T. Ranner, and C. Venkataraman. Coupled bulk-surface free boundary problems arising from a mathematical model of receptor-ligand dynamics. *SIAM J. Math. Anal.*, 49(1):360–397, 2017.

[12] I. Epstein and B. Xu. Reaction-diffusion processes at the nano- and microscales. *Nature Technology*, 11:312–319, 2016.

[13] PDE FlexPDE. Solutions inc. *URL http://www. pdesolutions. com*, 2015.

[14] A. Gierer. Generation of biological patterns and form: some physical, mathematical, and logical aspects. *Progress in biophysics and molecular biology*, 37:1–47, 1981.

[15] A. Gierer and H. Meinhardt. A theory of biological pattern formation. *Kybernetik*, 12(1):30–39, 1972.

[16] D. Gomez, S. Iyaniwura, F. Paquin-Lefebvre, and M. J. Ward. Pattern forming systems coupling linear bulk diffusion to dynamically active membranes or cells. *Phil. Trans. Roy. Soc. A.*, 379:20200276, 2021.

[17] A. Gomez-Marin, J. Garcia-Ojalvo, and J. M. Sancho. Self-sustained spatiotemporal oscillations induced by membrane-bulk coupling. *Phys. Rev. Lett.*, 98:168303, 2007.

[18] J. Gou, W.-Y. Chiang, P.-Y. Lai, M. J. Ward, and Y. X. Li. A theory of synchrony by coupling through a diffusive chemical signal. *Physica D*, 339:1–17, 2017.

[19] J. Gou, Y. X. Li, W. Nagata, and M. J. Ward. Synchronized oscillatory dynamics for a 1-D model of membrane kinetics coupled by linear bulk diffusion. *SIAM J. Appl. Dyn. Sys.*, 14(4):2096–2137, 2015.

[20] J. Gou and M. J. Ward. An asymptotic analysis of a 2-D model of dynamically active compartments coupled by bulk diffusion. *J. Nonlin. Sci.*, 26(4):979–1029, 2016.

[21] J. Gou and M. J. Ward. Oscillatory dynamics for a coupled membrane-bulk diffusion model with Fitzhugh-Nagumo kinetics. *SIAM J. Appl. Math.*, 76(2):776–804, 2016.

[22] S. Güttel and F. Tisseur. The nonlinear eigenvalue problem. *Acta Numerica*, 26(1):1–94, 2017.

[23] P. Haas and R. Goldstein. Turing's diffusive threshold in random reaction-diffusion systems. *Phys. Rev. Lett.*, 126:238101, 2021.

[24] J. Halatek, F. Brauns, and E. Frey. Self-organization principles of intracellular pattern formation. *Phil. Trans. R. Soc. B*, 373(1747):20170107, 2018.

[25] J. Halatek and E. Frey. Rethinking pattern formation in reaction–diffusion systems. *Nature Physics*, 14(5):507, 2018.

[26] S. Iyaniwura, J. Gou, and M. J. Ward. Synchronous oscillations for a coupled cell-bulk PDE-ODE model with localized cells on $\mathbb{R}^2$. *J. Eng. Math.*, 127(18):24 pp., 2021.

[27] S. Iyaniwura and M. J. Ward. Asymptotic analysis for the mean first passage time in finite or spatially periodic 2-D domains with a cluster of small traps. *ANZIAM*, 63(1):1–22, 2021.

[28] S. Iyaniwura and M. J. Ward. Synchrony and oscillatory dynamics for a 2-D PDE-ODE model of diffusion-mediated communication between small signalling compartments. *SIAM J. Appl. Dyn. Sys.*, 20(1):438–499, 2021.

[29] V. Klika, R. E. Baker, D. Headon, and E. A. Gaffney. The influence of receptor-mediated interactions on reaction-diffusion mechanisms of cellular self-organization. *Bull. Math. Bio.*, 74:935–957, 2012.

[30] K. Korvasová, Gaffney E. A., Maini P. K., Ferreira M. A., and V. Klika. Investigating the Turing conditions for diffusion-driven instability in the presence of a binding immobile substrate. *J. Theor. Biol.*, 367:286–295, 2015.

[31] A. Krause, E. A. Gafney, P. Maini, and V. Klika. Modern perspectives on near-equilibrium analysis of Turing systems. *Phil. Trans. R. Soc. A.*, 379:20200268, 2021.

[32] A. Landge, B. M. Jordan, X. Diego, and P. Müller. Pattern formation mechanisms of self-organizing reaction-diffusion systems. *Dev Biol.*, 460(1):2–11, 2020.

[33] I. Lengyel and I. R. Epstein. Modeling of Turing structures in the chlorite-iodide-malonic acid-starch reaction system. *Science*, 251:650, 1991.

[34] H. Levine and W. J. Rappel. Membrane-bound Turing patterns. *Phys. Rev. E*, 72:061912, 2005.

[35] A. Madzvamuse and A. H. W. Chung. The bulk-surface finite element method for reaction-diffusion systems on stationary volumes. *Finite Elem. Anal. Design*, 108:9–21, 2016.

[36] A. Madzvamuse, A. H. W. Chung, and C. Venkataraman. Stability analysis and simulations of coupled bulk-surface reaction-diffusion systems. *Proc. R. Soc., Ser. A*, 471(2175):20140546, 2015.

[37] P. Maini, K. Painter, and H. N. P. Chau. Spatial pattern formation in chemical and biological systems. *J. Chem. Soc. Faraday Trans.*, 93(1):3601–3610, 1997.

[38] L. Marcon, X. Diego, J. Sharpe, and P. Müller. High throughput mathematical analysis identifies Turing networks for patterning with equal diffusing signals. *eLife*, 5:e14022, 2016.

[39] P. Müller, K. W. Rogers, S. R. You, M. Brand, and A. F. Schier. Morphogen transport. *Development*, 140(8):1621–1639, 2013.

[40] F. Paquin-Lefebvre, W. Nagata, and M. J. Ward. Pattern formation and oscillatory dynamics in a two-dimensional coupled bulk-surface reaction-diffusion system. *SIAM J. Appl. Dyn. Syst.*, 18(3):1334–1390, 2019.

[41] F. Paquin-Lefebvre, W. Nagata, and M. J. Ward. Weakly nonlinear theory for oscillatory dynamics in a one-dimensional PDE-ODE model of membrane dynamics coupled by a bulk diffusion field. *SIAM J. Appl. Math.*, 80(3):1520–1545, 2020.

[42] F. Paquin-Lefebvre, B. Xu, K. L. DiPietro, A. E. Lindsay, and A. Jilkine. Pattern formation in a coupled membrane-bulk reaction-diffusion model for intracellular polarization and oscillations. *J. Theor. Biol.*, 497:110242, 2020.

[43] J. Pearson. Pattern formation in a (2+1)-species activator-inhibitor immobilizer system. *Physica A*, 188(1-3):178–189, 1992.

[44] J. Pearson and W. Horsthemke. Turing instabilities with nearly equal diffusivities. *J. Chem. Phys.*, 90:1588, 1989.

[45] M. Pelz and M. J. Ward. The emergence of spatial patterns for compartmental reaction kinetics coupled by two bulk diffusing species with comparable diffusivities. *Phil. Trans. Roy. Soc. A (38 pages, submitted)*, 2022.

[46] A. Rätz and M. Röger. Turing instabilities in a mathematical model for signaling networks. *J. Math. Biol.*, 65(6-7):1215–1244, 2012.

[47] A. Rätz and M. Röger. Symmetry breaking in a bulk–surface reaction–diffusion model for signalling networks. *Nonlinearity*, 27(8):1805, 2014.

[48] Andreas Rätz. Turing-type instabilities in bulk–surface reaction–diffusion systems. *J. Comp. Appl. Math.*, 289:142–152, 2015.

[49] E. M. Rauch and M. M. Millonas. The role of trans-membrane signal transduction in Turing-type cellular pattern formation. *J. Theor. Biol.*, 226(4):401–407, 2004.

[50] W. Ridgway, M. J. Ward, and B. T. Wetton. Quorum-sensing induced transitions between bistable steady-states for a cell-bulk ODE-PDE model with Lux intracellular kinetics. *J. Math. Bio.*, 84(1-2), 2021.

[51] B. Sozen, J. Cornwall-Scoones, and M. Zernicka-Goetz. The dynamics of morphogenesis in stem cell-based embryology: Novel insights for symmetry breaking. *Development*, 474:82–90, 2021.

[52] L. M. Stolerman, M. Getz, S. Llewellyn Smith, M. Holst, and P. Rangamani. Stability analysis of a bulk-surface reaction model for membrane protein clustering. *Bull. Math. Bio.*, 82(2), 2020.

[53] A. F. Taylor, M. Tinsley, and K. Showalter. Insights into collective cell behavior from populations of coupled chemical oscillators. *Phys. Chemistry Chem Phys.*, 17(31):20047–20055, 2015.

[54] A. F. Taylor, M. Tinsley, F. Wang, Z. Huang, and K. Showalter. Dynamical quorum sensing and synchronization in large populations of chemical oscillators. *Science*, 323(5914):614–6017, 2009.

[55] M. R. Tinsley, A. F. Taylor, Z. Huang, and K. Showalter. Emergence of collective behavior in groups of excitable catalyst-loaded particles: Spatiotemporal dynamical quorum sensing. *Phys. Rev. Lett.*, 102:158301, 2009.

[56] M. R. Tinsley, A. F. Taylor, Z. Huang, F. Wang, and K. Showalter. Dynamical quorum sensing and synchronization in collections of excitable and oscillatory catalytic particles. *Physica D*, 239(11):785–790, 2010.

[57] N. Tompkins, N. Li, C. Girabwe, and S. Fraden. Testing Turing's theory of morphogenesis in chemical cells. *PNAS*, 111(12):4397–4402, 2014.

[58] A. M. Turing. The chemical basis of morphogenesis. *Phil. Trans. Roy. Soc., Series B*, 237(641):37–72, 1952.

[59] V. K. Vanag and I. R. Epstein. Localized patterns in reaction-diffusion systems. *Chaos*, 17(3):037110, 2007.

[60] M. J. Ward. Spots, traps, and patches: Asymptotic analysis of localized solutions to some linear and nonlinear diffusive processes. *Nonlinearity*, 31(8):R189, 2018.

[61] B. Xu and P. Bressloff. A PDE-DDE model for cell polarization in fission yeast. *SIAM J. Appl. Math.*, 76(3):1844–1870, 2016.

[62] B. Xu and A. Jilkine. Modeling the dynamics of Cdc42 oscillation in fission yeast. *Biophysical J.*, 114(3):711–722, 2018.